The Journal of Chemical Physics

RESEARCH ARTICLE | JANUARY 17 2023

Understanding dynamics in coarse-grained models. I. Universal excess entropy scaling relationship

Jaehyeok Jin ; Kenneth S. Schweizer ; Gregory A. Voth

J. Chem. Phys. 158, 034103 (2023)
https://doi.org/10.1063/5.0116299

AIP Publishing

The Journal of Chemical Physics ARTICLE scitation.org/journal/jcp

Understanding dynamics in coarse-grained models. I. Universal excess entropy scaling relationship

Cite as: J. Chem. Phys. 158, 034103 (2023); doi: 10.1063/5.0116299
Submitted: 28 July 2022 • Accepted: 27 October 2022 •
Published Online: 17 January 2023

Jaehyeok Jin,[1] Kenneth S. Schweizer,[2] and Gregory A. Voth[1,a)]

AFFILIATIONS

[1] Department of Chemistry, Chicago Center for Theoretical Chemistry, Institute for Biophysical Dynamics, and James Franck Institute, The University of Chicago, Chicago, Illinois 60637, USA
[2] Department of Material Science, Department of Chemistry, Department of Chemical and Biomolecular Engineering, and Materials Research Laboratory, University of Illinois, Urbana, Illinois 61801, USA

[a)] **Author to whom correspondence should be addressed:** gavoth@uchicago.edu

ABSTRACT

Coarse-grained (CG) models facilitate an efficient exploration of complex systems by reducing the unnecessary degrees of freedom of the fine-grained (FG) system while recapitulating major structural correlations. Unlike structural properties, assessing dynamic properties in CG modeling is often unfeasible due to the accelerated dynamics of the CG models, which allows for more efficient structural sampling. Therefore, the ultimate goal of the present series of articles is to establish a better correspondence between the FG and CG dynamics. To assess and compare dynamical properties in the FG and the corresponding CG models, we utilize the excess entropy scaling relationship. For Paper I of this series, we provide evidence that the FG and the corresponding CG counterpart follow the same universal scaling relationship. By carefully reviewing and examining the literature, we develop a new theory to calculate excess entropies for the FG and CG systems while accounting for entropy representability. We demonstrate that the excess entropy scaling idea can be readily applied to liquid water and methanol systems at both the FG and CG resolutions. For both liquids, we reveal that the scaling exponents remain unchanged from the coarse-graining process, indicating that the scaling behavior is universal for the same underlying molecular systems. Combining this finding with the concept of mapping entropy in CG models, we show that the missing entropy plays an important role in accelerating the CG dynamics.

I. INTRODUCTION

With the aid of computation, coarse-grained (CG) models allow for an efficient exploration of accessible spatiotemporal scales occurring in chemical and physical systems.[1–10] This enhancement is feasible by integrating out fast degrees of freedom at the fine-grained (FG) resolution, thus extending the applicability of computer simulations to larger system sizes and longer simulation times than was previously perceived to be possible (for example, from HIV-1 research; see Refs. 11–15). To reproduce equilibrium structural correlations in CG models compared to the FG reference, various bottom-up CG methods have been proposed to approximate the potential of mean force (PMF) between the CG particles as the effective CG interaction.[1–10,16–20] Since the static equilibrium correlations can be well-captured by designing these conservative interactions between CG particles, bottom-up CG simulations are generally carried out with Newtonian dynamics having only conservative forces. During this CG Newtonian mechanics, the CG configuration space tends to have a flatter or softer effective potential energy surface than that of the FG reference, resulting in faster diffusion dynamics than in the FG dynamics.[21–26] While this artificial "acceleration" helps to extend the sampling of the CG simulation, it hinders the study of explicitly dynamical properties with the CG model. It is known from the Mori–Zwanzig formalism[27–30] that this acceleration in the CG model occurs due to missing fluctuation and dissipation forces in the CG equations of motion, but there is no alternative theory to qualitatively understand the physical nature of these missing forces and to quantitatively estimate the degree of the acceleration in the CG model over the FG one due to the absence of fluctuation and dissipation forces.

In this light, numerous approaches and theories have been developed and applied to understand the CG dynamics with respect to the reference FG dynamics. Briefly, using the projection operator technique of Zwanzig,[27–30] one can show that the time evolution of specific collective variables in the reduced phase space follows the form of the Generalized Langevin Equation (GLE). Therefore, in an ideal sense, dynamics in the reduced CG representation could be faithfully represented by the Mori–Zwanzig formalism. Despite its theoretical rigor, a full derivation of Mori–Zwanzig equations of motion for the CG system would be highly challenging or even intractable without making approximations to specify the non-Markovian frictional and fluctuation forces, which in turn are completely dependent on the nature of the system.[23,31] While we are aware of numerous efforts to emulate both the structural and dynamical properties of CG systems based on the Mori–Zwanzig formalism, e.g., works from Español, Karniadakis, and others,[23,25,26,32–47] we instead focus here on the CG Newtonian mechanics and aspire to better understand and to better characterize the acceleration behavior of the CG system over the FG one from which it is derived.

In the literature, several researchers have proposed a time-rescaling approach where the time step in CG simulations is effectively rescaled to match some reference dynamical behavior.[24,48–50] While time-rescaling offers a reasonably intuitive and sometimes applicable approach, there are intrinsic drawbacks such that the scaling behavior is not universal among different systems.[51–54] In order to exactly determine the rescaling factor, one may need to revisit the GLE or Langevin equation to estimate the frictional forces.[35] A comprehensive review of these distinct approaches to understand the dynamics of CG models is detailed in the literature.[55,56]

In this series of papers, we offer a different approach to assessing the dynamical properties of the CG system. This alternative approach is based on the excess entropy of the system. The relationship, known as "excess entropy scaling," posits that the dynamical properties of a system (especially self-diffusion) scale as the excess entropy of that system.[57–61] Even though suggesting that entropy as a thermodynamic quantity is related to the system dynamics seems counterintuitive at first glance based on fundamental statistical mechanics,[62] this semi-quantitative relation has been established to be useful under certain systems:[63] Starting from the original work for the Lennard–Jones and soft-sphere models,[57] the excess entropy scaling formalism has been demonstrated in many complex systems, such as liquid metals,[64,65] ionic liquids,[66] polymer chains,[67] and even extended to confined systems.[68,69] We note that these "liquid" systems are at ambient (or normal liquid, not deeply supercooled, regime) conditions at relatively high temperatures that do not exhibit strong activated dynamics. Given its apparent validity in a number of physical systems, several theoretical developments have provided some physical explanations underlying the excess entropy scaling relationship. As hinted by mode coupling theory (MCT),[70,71] which links structures and dynamics based on the radial distribution function (RDF),[72,73] recent work has further suggested that the phenomenological entropy scaling can be microscopically derived in certain conditions.[74] In addition, other theoretical connections between the Kolmogorov–Sinai entropy and dynamical properties are described in the literature.[73–77] It should be noted that recent findings suggest that one can possibly derive the scaling relationship in simple Hamiltonian systems using Boltzmann's formula and rate theory.[61] Yet, there appears to be no systematic, first-principles theory to fully derive the excess entropy scaling relationship in any Hamiltonian system to date.

Interestingly, relatively less attention has been given to applications of excess entropy scaling to CG models, and therefore, it is of particular interest to systematically extend this relationship to CG dynamics. While earlier work provided somewhat limited interpretations[78] or implications for the relative entropy formalism of simple models,[79] recent research efforts to apply the excess entropy scaling to CG models have been reported,[80,81] hinting that a rigorous extension to CG systems may be feasible. However, two main caveats have limited the application of this concept to CG modeling. First and foremost, despite its applicability for a wide range of molecular systems, there is no guarantee that such a scaling relationship still holds for CG systems. More importantly, even if it does hold, no systematic theories or studies have shown that both FG and corresponding CG systems will exhibit the same (universal) scaling behavior. Without confirming the universality between FG and its corresponding CG systems, an effort that tries to understand CG dynamics in terms of excess entropy scaling would be difficult. In particular, the aforementioned drawbacks are due to the empirical nature of the scaling relationship, and thus, the physical understanding and correspondence between full FG dynamics and CG dynamics are still premature and largely unexplored.

In this series of papers, we aim to deliver a more comprehensive understanding of CG dynamics with respect to the underlying FG dynamics. For Paper I of the series, we will introduce the concept of excess entropy scaling for the FG system and then also the corresponding CG system by developing a new method to correctly address different modal contributions to excess entropy. Then, we will determine the excess entropy of atomistic systems and their CG counterparts based on entropy representability. After confirming that the excess entropy scaling relationship holds, in general, we will explore if the same scaling relationship holds for both the FG and CG dynamics for the same molecular system in order to elucidate the universal nature of excess entropy scaling in such systems.

II. THEORY

A. Excess entropy scaling relationship

The starting point for the scaling relationship is to define the excess entropy of the system at a given number density ρ and temperature T such that

$$S_{ex} = S_{ex}(\rho, T) := S(\rho, T) - S_{\mathrm{id}}(\rho, T), \tag{1}$$

where $S(\rho, T)$ is the system entropy, and $S_{\mathrm{id}}(\rho, T)$ is the corresponding ideal gas entropy with the same ρ and T. Since the ideal gas is the maximally disordered state, this condition gives $S_{ex} < 0$ for non-ideal systems. The excess entropy scaling aims to connect this thermodynamic property to a reduced dynamic quantity, such as the self-diffusion coefficient. Two distinct scaling schemes have been suggested, and here, both are introduced and compared comprehensively.

First, the most well-known scaling relationship, known as the Rosenfeld scaling, is given by[57–59]

$$D^* = D_0 \exp(\alpha S_{ex}/Nk_B), \tag{2}$$

where the reduced dynamic property (diffusion coefficient in this case) is scaled as

$$D^* = D\frac{\rho^{\frac{1}{3}}}{(k_BT/m)^{\frac{1}{2}}}. \tag{3}$$

Here, α and D_0 are the coefficients obtained from the scaling relationship and are dependent on the system of interest. Alternatively, Dzugutov reported a similar relationship expressed by a slightly different formalism,[60]

$$D_Z^* = D_Z^0\ \exp(S_{ex}^{(2)}/Nk_B), \tag{4}$$

where $S_{ex}^{(2)}$ is the two-body contribution to the full excess entropy S_{ex}, including multi-particle correlations. Even though Eqs. (2) and (4) look similar at first glance, the two scaling schemes have distinct D_0 and α expressions. Such differences between the Rosenfeld and Dzugutov scaling schemes are extensively discussed in the literature, but here, we emphasize the key differences and determine which scheme is more physically appropriate for the scope of this work. First, in Eq. (4), the diffusion coefficient is reduced by $D_Z^* = D\cdot(\sigma^{-2}\Gamma_E^{-1})$ using the Enskog theory for hard spheres with the collision frequency of $\Gamma_E = 4\pi\sigma^2\rho g(\sigma)\sqrt{k_BT/(\pi m)}$. The idea of using the microscopic Enskog collision rate is because the Dzugutov scaling was derived by assuming that the diffusion process can be regarded as a molecular "caging" effect in hard spheres.[60] In this sense, the exponent in the Dzugutov scaling becomes unity ($\alpha = 1$) under the ergodic assumption, but this scaling may only be valid in hard sphere diffusion processes. We note that recent work demonstrated that this ergodic assumption is usually not satisfied in many Molecular Dynamics (MD) simulations,[82] and an alternative exponent 2/3 was instead derived in the case of the Dzugutov scaling from the MCT.[72] On the other hand, the Rosenfeld scaling applies to many dynamic properties, including diffusion, viscosity, and thermal conductivity, indicating that the Dzugutov scaling is less universal and less globally accurate than the Rosenfeld scaling, as has been pointed out by several researchers.[83]

The physical consistency can also be seen from the scaling coefficient. In Eq. (3), the diffusion coefficient is scaled by elementary quantities (the so-called macroscopically reduced units) that correspond to the characteristic length and timescales in Newtonian dynamics. In theory, the reduced units applied in Eq. (3) are equivalent to the reduced quantities used in the isomorph theory of Dyre, implying a hidden scale invariance of strongly correlating systems, which can explain the quasi-universality of scaling relationships.[84,85] On the other hand, the reduced unit in the Dzugutov scaling is rather microscopic and empirical, and this scaling scheme may be dubious in some cases where diverging behavior is observed.[77]

Finally, the excess entropy terms utilized in these two scaling relationships are different. The Dzugutov scaling only utilizes the pair excess entropy term $S_{ex}^{(2)}$, while the other contributions are neglected, whereas the Rosenfeld scaling employs the overall excess entropy of the system S_{ex} to better capture the full entropy contribution.

To summarize, in this series of papers, we follow the original scaling idea from the work of Rosenfeld using the macroscopically reduced units for both FG and CG systems since it is a more general scaling relation for liquids and also consistent with a macroscopic point of view. However, a physical idea behind the Dzugutov scaling, the Enskog picture, will be revisited in Paper II.[176] With this in mind, we aim to relate the FG diffusion relationship based on the Rosenfeld excess entropy scaling,

$$D_{\mathrm{FG}}^* = D_0^{\mathrm{FG}}\ \exp(\alpha^{\mathrm{FG}}s_{ex}^{\mathrm{FG}}), \tag{5}$$

to its CG counterpart,

$$D_{\mathrm{CG}}^* = D_0^{\mathrm{CG}}\ \exp(\alpha^{\mathrm{CG}}s_{ex}^{\mathrm{CG}}), \tag{6}$$

where we denote the per particle entropy as $s_{ex} = S_{ex}/Nk_B$ for simplicity. In other words, the main goal of this paper is to determine α^{FG} and α^{CG} by calculating s_{ex}^{FG} and s_{ex}^{CG} to probe whether the CG scaling relationship follows the same scaling exponent. The theories behind the calculation of s_{ex}^{FG} and s_{ex}^{CG} are presented in Secs. II B and II C.

B. Excess entropy estimation

1. Conventional approach: Multiparticle correlation expansion

Substantial research effort has focused on the means for calculating excess entropy. In principle, a direct determination of excess entropy is possible by separately calculating the system entropy and the ideal gas entropy using conventional methods, e.g., thermodynamic integration (TI). Although we are aware of many papers that have employed TI to calculate excess entropies,[86–88] we opt not to use this method in this work because TI is less straightforward for linking the thermodynamics and structures between the detailed (FG) systems to their reduced (CG) version. We seek to utilize a more straightforward method that can physically elucidate the missing degrees of freedom during the coarse-graining process in order to estimate excess entropy. Additionally, there are several practical concerns of conventional TI calculations: (1) design of a corresponding ideal gas system is needed and (2) slow numerical convergence of the method.

Instead of the TI method, a configuration-based approach to calculating the excess entropy quantity can be designed based on statistical mechanical theory. From Green's derivation of multiparticle correlation functions,[89] Wallace rederived a systematic expansion of the excess entropy expressed as a sum of integrals of n-particle distribution functions,[90–93]

$$S_{ex} = \sum_{n\geq 2} S^{(n)}. \tag{7}$$

In Eq. (7), $S^{(n)}$ is the excess entropy contribution from the n-particle contributions. The simplest and most common approach to evaluating S_{ex} is to approximate the two-body contribution as being dominant compared to other higher-order contributions, as shown in several theoretical derivations.[89,94–96] Furthermore, for a variety of systems, this assumption has been widely adopted due to the fact that the $S^{(3)}$ term cancels other higher-order contributions.[66,97–100] With this in mind, the $S^{(2)}$ term is written as a function from the pair distribution function $g^{(2)}(\mathbf{r})$,

$$S^{(2)} = -2\pi\int_0^\infty \left\{g^{(2)}(\mathbf{r})\ln g^{(2)}(\mathbf{r}) - \left[g^{(2)}(\mathbf{r})-1\right]\right\}\mathbf{r}^2\cdot d\mathbf{r}, \tag{8}$$

where the vector $\mathbf{r}$ includes information about both the position and orientation of the molecule. Namely, Eq. (8) provides a configurational basis to estimate excess entropy for various systems of interest.

2. Orientational contribution

An important point to note in Eq. (8) is that the pair distribution function $g^{(2)}(\mathbf{r})$ is a function of not only the pair distance between particles $r = |\mathbf{r}|$ but also positions of the particle pair $\mathbf{r}_1$ and $\mathbf{r}_2$ with their orientations ω_1 and ω_2, resulting in 12 variables. However, the majority of current literature only considers the translational component while ignoring the orientational (or angular) contribution when calculating the scalar term,[101]

$$S^{(2)}_{\text{trans}} = -2\pi\rho \int_0^\infty \left\{ g^{(2)}(r) \ln g^{(2)}(r) - \left[g^{(2)}(r) - 1 \right] \right\} r^2 \cdot dr. \quad (9)$$

It is straightforward to see that Eq. (9) corresponds to only the translational component because the orientational dependence on ω_1 or ω_2 no longer appears. Since only the RDF is required, this choice is more numerically feasible and often preferred. Furthermore, the so-called "homogeneity assumption"[67] whereby S_2 contributes nearly 80% to the overall excess entropy is satisfied by simple models where there are no orientational degrees of freedom, e.g., Lennard-Jones fluids.[102,103] However, as Malvaldi and Chiappe have noted, this approximation is often violated when the molecule has non-spherical symmetry.[66] Thus, in the case of water and methanol studied in the present work, such considerations need to be carefully addressed. In particular, many studies reported calculating the excess entropy of water to understand its connection to anomalous properties.[86,104–107] Subsequently, two pertinent findings were discovered: (1) the contribution of non-translational components in water is large[108–112] and (2) the orientational entropy is not explicitly connected to the translational entropy,[113] meaning that translational entropy based on the RDF cannot account for orientational contributions. Altogether, we believe that having only translational components from the RDF to calculate the excess entropy can incur major errors.

In that light, several theories and computational techniques have been devised to account for the orientational contributions beyond the pair translational motion. For rigid molecules, Lazaridis and Karplus suggested that the function $g^{(2)}(\boldsymbol{r}_{12})$ can be factorized as follows:[109]

$$g^{(2)}(\boldsymbol{r}_{12}) = g^{(2)}(r, \omega_1, \omega_2) = g^{(2)}_{\text{trans}}(r) \cdot g^{(2)}_{\text{or}}(\omega_1, \omega_2 | r). \quad (10)$$

Later, Zielkiewicz[108] designed a slightly different factorization scheme in terms of translational, configurational, and orientational contributions in order to perform feasible integrations,

$$g^{(2)}(\boldsymbol{r}_{12}) = g^{(2)}(r, \omega_1, \omega_2) = g^{(2)}_{\text{trans}}(r) \cdot g^{(2)}_{\text{conf}}(\omega_1 | r) \cdot g^{(2)}_{\text{orient}}(\omega_2 | r, \omega_1). \quad (11)$$

Equations (10) and (11) separate the translational component from the orientational contribution using a conditional probability distribution function. However, a direct calculation of configurational and orientational correlations of molecular pairs in liquids is numerically challenging due to the multi-dimensional numerical integrations. To elaborate, this orientational contribution is characterized by the following integration form:

$$S^{(2)}_{\text{or}} = -2\pi\rho \int_0^\infty g^{(2)}(r) \cdot \left(-\frac{1}{\Omega^2} \iint J(\omega_1, \omega_2) g(\omega_1, \omega_2 | r) \times \ln g(\omega_1, \omega_2 | r) d\omega_1 d\omega_2 \right) dr, \quad (12)$$

where $\Omega = \int d\omega = 8\pi^2$, and $J(\omega_1, \omega_2)$ is the Jacobian of the angular variables ω_1, ω_2. Under homogeneous and isotropic conditions, we can reduce the angular variables to five[109] or six angles[108] depending on the choice of factorization. However, a full calculation of such collective integrations over both distance and orientational variables is numerically very demanding.[78,108,114,115] Even though several algorithmic improvements have been proposed after Lazaridis, Karplus, and Zielkiewicz,[116,117] only a few follow-up reports are available in the literature to date. Yet, these approaches emphasize that one must consider more than just the translational contribution, especially in water.

3. Alternative approach: 2PT-based method

To surmount the numerical challenges mentioned earlier, we use the two-phase thermodynamic (2PT) method[118–122] that has been applied to various chemical systems[123–127] as an alternative approach. Herein, we provide essential steps in performing the 2PT simulation, with more detailed derivations and discussion found in Refs. 118–122. In a nutshell, the 2PT method constructs the partition function of the system by designing the density of the states (DoS) of the system as a linear combination of solid-like and gas-like (diffusive) components. The total DoS of liquid is usually obtained from the Fourier transform of the velocity autocorrelation function (VACF) $C_{vv}(t)$,

$$\text{DoS}_{\text{liq}}(\nu) = \lim_{\tau \to \infty} \frac{1}{2k_B T} \int_{-\tau}^{\tau} C_{vv}(t) e^{-2\pi\nu t} dt, \quad (13)$$

where ν denotes the frequency of normal modes. This allows for decomposing the liquid DoS into a fully harmonic solid-like component and an anharmonic diffusive component with weights $\omega(\nu)$,

$$\text{DoS}_{\text{liq}}(\nu) = \omega_{\text{solid}}(\nu) \text{DoS}_{\text{solid}}(\nu) + \omega_{\text{gas}}(\nu) \text{DoS}_{\text{gas}}(\nu). \quad (14)$$

Detailed formulas for $\omega_{\text{solid}}(\nu)$ and $\omega_{\text{gas}}(\nu)$ can be found in the original 2PT literature.[118–122] From the decomposed liquid DoS in Eq. (14), the corresponding thermodynamic entropy can be calculated using the entropy weighing function $W(\nu)$ for solid and gas phases. For example, the gas component as a hard sphere system such that the gas-like weights $W_{\text{gas}}(\nu)$ are readily given as a function of the hard sphere entropy. The $\text{DoS}_{\text{gas}}(\nu)$ term is then calculated by solving the fluidity term in the gas-like DoS by matching the diffusivity of the system to the Carnahan–Starling equation of state. Finally, the solid-like weight $W_{\text{solid}}(\nu)$ is assumed to be a harmonic oscillator : $W_{\text{solid}}(\nu) = \frac{\beta\hbar\nu}{\exp(\beta\hbar\nu)-1} - \ln[1 - \exp(-\beta\hbar\nu)]$.

This basic approach of 2PT is then applied to the primary degrees of freedom in the molecular frame in order to decompose thermodynamic properties into different modal contributions. In

other words, the overall velocity of molecules can be decomposed in the same manner,

$$v(t) = v_{\text{trans}}(t) + v_{\text{rot}}(t) + v_{\text{vib}}(t). \tag{15}$$

While the translational velocity corresponds to the center-of-mass motion, the rotational velocity can be determined from the angular velocity $\omega(t)$ based on the definition of the angular momentum $L = \mathbf{I}\omega$. By inverting the inertia tensor $\mathbf{I}$, one could estimate $\omega(t)$, and then, the angular velocity $v_{\text{rot}}(t)$ is computed as $v_{\text{rot}}(t) = \omega(t) \times r(t)$. Having these two components in hand, the vibrational velocity $v_{\text{vib}}(t)$ is readily obtained as a complement: $v_{\text{vib}}(t) = v(t) - (v_{\text{trans}}(t) + v_{\text{rot}}(t))$. Then, the thermodynamic quantities corresponding to each motion are calculated based on Eq. (14). Assuming this general decomposition of atomistic velocities, the overall entropy of the system can be decomposed into translational, rotational, and vibrational components as[118–127]

$$S = S_{\text{trans}} + S_{\text{rot}} + S_{\text{vib}}. \tag{16}$$

Each entropy component ($t \cup r \cup v$ indicating each modal contribution, respectively) is calculated by

$$S_{t\cup r\cup v} = k_B\left[\int_0^\infty W_{\text{solid}}^{t\cup r\cup v}(\nu)\text{DoS}_{\text{solid}}^{t\cup r\cup v}(\nu) + \int_0^\infty W_{\text{gas}}^{t\cup r\cup v}(\nu) \times \text{DoS}_{\text{gas}}^{t\cup r\cup v}(\nu)d\nu\right], \tag{17}$$

meaning that one must determine $W_{\text{solid}}^{t\cup r\cup v}(\nu), \text{DoS}_{\text{solid}}^{t\cup r\cup v}(\nu)$, $W_{\text{gas}}^{t\cup r\cup v}(\nu)$, and $\text{DoS}_{\text{gas}}^{t\cup r\cup v}(\nu)$. First, translational entropy is calculated using the center-of-mass velocities to construct the $\text{DoS}_{\text{liq}}^{\text{COM}}(\nu)$ and to apply the aforementioned procedures to yield $W_{\text{solid}}^{\text{COM}}(\nu)$ and $W_{\text{gas}}^{\text{COM}}(\nu)$. For the rotational components, we repeat the calculation using $v_{\text{rot}}(t) = \omega(t) \times r(t)$. Finally, the vibrational entropy is computed solely from the solid-like contributions of the harmonic oscillators.

The partition scheme that 2PT provides as translational, rotational, and vibrational contributions is also consistent with the partition scheme used in Eqs. (10) and (11). We envisage that the translational contribution remains the same, while the rotational and vibrational components complement the orientational entropies. Moreover, the 2PT partition scheme, Eq. (16), allows for differentiating the missing modes from the coarse-graining procedure. It is worth noting that we recently elucidated the missing entropies during the coarse-graining process for the single-site CG model using this framework.[128] Here, single-site CG models are represented as the center-of-mass of each molecule, which interact via isotropic CG pair potentials. At this CG resolution, assessing the missing entropy is much more intuitive since the CG system has only translational motions. The entropy representability relationship further suggests that the translational components from the FG entropy remain at the CG resolution, while other entropies from rotation and vibration are mapped into the approximate CG PMF.[128] A theoretical link between the missing entropy and excess entropy scaling was first suggested in Ref. 79 using an idea of relative entropy, where it was postulated that the relative entropy differences are responsible for differences in dynamics if the scaling relationship in both models holds with the same scaling exponent. However, in their work,[79] this hypothesis was originally suggested for analytically mapping Lennard-Jones liquids to simple soft-sphere potentials at the same resolution and was never rigorously verified for actual molecular systems upon a coarse-graining process.

Despite the 2PT receiving less attention in the literature for the calculation of excess entropy, a few examples have successfully demonstrated its applicability. To our knowledge, employing the 2PT-based approach for the atomistic liquid systems was first introduced by Dhabal *et al.*,[107] and then Palomar and Sesé separately demonstrated the 2PT-based approach for atomistic dipolar liquids.[129] More importantly, these two distinct efforts were able to show that the 2PT-based excess entropy reproduces trends as accurately as from the TI values, thus validating its feasibility in computing excess entropy. Similarly, work from Bernhardt *et al.* utilized the 2PT method as an extension of Ref. 128 to obtain the translational excess entropies in a CG model.[81] Both papers illustrated that the 2PT method could be used to calculate the excess entropy of the CG system; however, the aforementioned attempts were only limited to translational motion in the center-of-mass frame. We note that considering only a translational component to the excess entropy ignores contributions from other motions at resolutions finer than the single-site CG, resulting in incorrect scaling relationship and dynamics. The α exponent near 0.38 in Eq. (2) for CG systems was underestimated as reported in Ref. 81. This value suggests that one needs to fully consider the representative motions at the CG level. Inspired by this inconsistency, we propose a full 2PT-based approach to calculating the excess entropy beyond the translational entropy for both the FG and its corresponding CG systems by addressing entropy representability. While one could recover the missing entropy values from CG simulations by utilizing entropy representability,[128] here, our intention is to elucidate the excess entropy differences between the FG and CG systems since most CG simulations with accelerated CG dynamics do not fully account for the missing entropy.

Our proposed approach utilizes the same partitioning used in the 2PT method. That is, we divide the FG system entropy into translational and angular terms,

$$S^{\text{FG}} = S_{\text{trn}}^{\text{FG}} + S_{\text{or}}^{\text{FG}} = S_{\text{trn}}^{\text{FG}} + S_{\text{rot}}^{\text{FG}} + S_{\text{vib}}^{\text{FG}}. \tag{18}$$

The first separation in Eq. (18) was from Eq. (10), and thus, the excess entropy at the FG model becomes

$$S_{ex}^{\text{FG}} = S^{\text{FG}} - S^{(\text{id})} = S_{\text{trn}}^{\text{FG}} + S_{\text{rot}}^{\text{FG}} + S_{\text{vib}}^{\text{FG}} - \left(S_{\text{trn}}^{(\text{id})} + S_{\text{rot}}^{(\text{id})} + S_{\text{vib}}^{(\text{id})}\right). \tag{19}$$

Likewise, the entropy of the corresponding single-site CG system can be formulated as

$$S^{\text{CG}} = S_{\text{trn}}^{\text{CG}}, \tag{20}$$

where the corresponding excess entropy is solely the translational contributions from Eq. (19), i.e.,

$$S_{ex}^{\text{CG}} = S^{\text{CG}} - S^{(\text{id})} = S_{\text{trn}}^{\text{CG}} - S_{\text{trn}}^{(\text{id})}. \tag{21}$$

To reiterate, the prior work in the literature has mainly attempted to employ Eq. (20) to determine excess entropy scaling, but here, we emphasize that one must also consider $S_{\text{rot}}^{\text{FG}} + S_{\text{vib}}^{\text{FG}}$ to correctly address the question of FG scaling. We will demonstrate this method for two different molecular systems in Secs. III C and III D.

C. Excess entropy formulation

1. Fine-grained system

From the definition of the excess entropy, the FG entropy can be obtained from a direct 2PT calculation, whereas the corresponding ideal gas entropy term can be written as an analytical formulation deduced from statistical mechanical theory.[130] Despite the FG resolution, the diffusion behavior is characterized by the trajectories of the mapped center-of-mass of each molecule. Therefore, the translational entropy must correspond to the single-component ideal gas, and this term can be readily obtained by employing the Sackur–Tetrode equation,

$$s_{\mathrm{trn}}^{(\mathrm{id})} = \frac{S_{\mathrm{trn}}^{(\mathrm{id})}}{Nk_B} = -\ln\left(\frac{h^2}{2\pi m k_B T}\right)^{\frac{3}{2}} - \ln\left(\frac{N}{V}\right) + \frac{5}{2}. \tag{22}$$

Even though the translational motions can be extracted from the center-of-mass entities, the rotational motions also contribute to the overall entropy of the system at the FG resolution. For an ideal gas, the rotational partition function for the specific rotational modes at a temperature Θ_r has the form

$$q_{\mathrm{rot}} = \frac{8\pi^2 I k_B T}{\sigma h^2} = \frac{T}{\sigma \Theta_r}. \tag{23}$$

The characteristic rotational temperatures are related to the moment of inertia with respect to the principal moments I_r: $\Theta_r = h^2/8\pi^2 k I_r$. From the rotational partition function, the corresponding ideal gas entropy term is given as

$$s_{\mathrm{rot}}^{(\mathrm{id})} = \frac{S_{\mathrm{rot}}^{(\mathrm{id})}}{Nk_B} = \ln\left[\frac{\sqrt{\pi}}{\sigma}\left(\frac{T^3 e^3}{\Theta_A \Theta_B \Theta_c}\right)^{\frac{1}{2}}\right], \tag{24}$$

where the rotations along the x, y, and z axes have rotational temperatures ordered as $\Theta_A \geq \Theta_B \geq \Theta_c$ with the rotational symmetry number σ.

The last term in Eq. (19) that corresponds to the vibrational contributions is computed from the polyatomic vibrational partition function,

$$q_{\mathrm{vib}} = \prod_j^{F_v} \frac{e^{-\Theta_{v_j}/2T}}{1 - e^{-\Theta_{v_j}/T}}, \tag{25}$$

where the characteristic vibration temperatures are similarly defined as $\Theta_{v_j} = h\nu_j/k$ by denoting ν_j as the characteristic frequency of the jth vibrational modes. F_v are the remaining degrees of freedom for the vibrational modes. For our work, $F_v = 3N - 6$ due to non-linearity. Altogether, q_{vib} determines the vibrational entropy of the ideal gas $s_{\mathrm{vib}}^{(\mathrm{id})}$,

$$s_{\mathrm{vib}}^{(\mathrm{id})} = \frac{S_{\mathrm{vib}}^{(\mathrm{id})}}{Nk_B} = \sum_{j=1}^{3N-6}\left[\frac{\Theta_{vj}/T}{e^{\Theta_{vj}/T} - 1} - \ln\left(1 - e^{-\Theta_{v_j}/T}\right)\right]. \tag{26}$$

However, vibrational contributions are generally known to be negligible compared to translational and rotational components. In particular, for FG water force fields, the oxygen–hydrogen bond is usually considered rigid. Therefore, the final excess entropy term used in this work is written as

$$s_{ex}^{\mathrm{FG}} = s^{\mathrm{FG}} - \left[\frac{5}{2} - \ln\left(\frac{h^2}{2\pi m k_B T}\right)^{\frac{3}{2}} - \ln\left(\frac{N}{V}\right)\right] - \ln\left[\frac{\sqrt{\pi}}{\sigma}\left(\frac{T^3 e^3}{\Theta_A \Theta_B \Theta_c}\right)^{\frac{1}{2}}\right]. \tag{27}$$

2. Coarse-grained system

Equation (21) is built upon the findings of Ref. 128 that the single-site CG model has only translational motions. Since the CG system is constructed under the same condition as the FG system, we can repeat Eq. (22) for the CG excess entropy s_{ex}^{CG} as

$$s_{ex}^{\mathrm{CG}} = s^{\mathrm{CG}} - \left[\frac{5}{2} - \ln\left(\frac{h^2}{2\pi m k_B T}\right)^{\frac{3}{2}} - \ln\left(\frac{N}{V}\right)\right]. \tag{28}$$

The CG excess entropy becomes fairly complicated when each molecule is mapped to more than two CG sites. In principle, one could include the rotational contribution to the CG excess entropy by extracting the angular velocity of the CG beads along with the computed moment of inertia tensor following the 2PT argument. We will estimate the CG excess entropy of the two-site CG system in the Appendix.

D. Coarse-grained model

1. CG water model: BUMPer

An accurate bottom-up CG model is designed to capture important structural correlations in the CG system.[8,131–133] Among a number of bottom-up CG methods, the multiscale coarse-graining (MS-CG) methodology is shown to capture up to three-body correlations using only two-body basis sets. Practically speaking, the MS-CG force fields are fitted to approximate the many-body PMF using variational force-matching. In this regard, CG water models often aim to capture three-body correlations in water that originate from hydrogen bonding.[134–136] However, in the force-matched CG water models, we recently found that the pairwise basis sets fail to reproduce structural correlations, unlike other simple liquids. An alternative approach is to utilize the CG water model based on the Stillinger–Weber (SW) interaction,[137] such as the mW model,[138] or the three-body force-matched CG model.[139,140] However, having a three-body interaction would slow down the overall performance of the CG model, and there have been studies indicating that the SW-based water model may be problematic for the entropy scaling due to its many-body nature.[64,141,142]

The aforementioned drawbacks can be mitigated by employing our recently developed bottom-up CG model, which we call the Bottom-Up Many-Body Projected Water (BUMPer) model.[143,144] We have shown that the BUMPer CG interaction faithfully corresponds to the CG interaction obtained from many-body projection theory. In brief, the many-body projection theory stems from the many-body expansion (MBE) of the CG interaction $U(\mathbf{R}^N)$,

$$U(\mathbf{R}^N) = \sum_I \sum_{J\neq I} U^{(2)}(R_{IJ}) + \sum_I \sum_{J\neq I} \sum_{K>J} U^{(3)}(\theta_{JIK}, R_{IJ}, R_{IK}) + \sum_{IJKL} U^{(4)}(\theta_1, \theta_2, \phi) + \cdots, \tag{29}$$

to effectively project higher-order interactions onto lower-order basis sets, which is similar to the Bogoliubov–Born–Green–Kirkwood–Yvon hierarchy in liquid state theory.[145–149] We applied

this theory by first performing force-matching up to three-body interactions[140] and then effectively projecting the force-matched three-body SW interaction $U^{(3)}(\theta_{JIK}, R_{IJ}, R_{IK})$, which is written as

$$U^{(3)}(\theta_{JIK}, R_{IJ}, R_{IK}) = \lambda_{JIK}(\cos\theta_{JIK} - \cos\theta_0)^2 \exp\left(\frac{\gamma_{IJ}}{R_{IJ} - \sigma_{IJ}}\right) \times \exp\left(\frac{\gamma_{IK}}{R_{IK} - \sigma_{IK}}\right), \quad (30)$$

onto the pairwise basis sets via

$$U(\mathbf{R}^N) = \sum_I \sum_{J\neq I} \left\{ U_{3b}^{(2)}(R_{IJ}) + 2(N_c - 1) \int d\theta_{JIK} dR_{IK} \times p(\theta_{JIK}, R_{IK}|R_{IJ}) U^{(3)}(\theta_{JIK}, R_{IJ}, R_{IK}) \right\}. \quad (31)$$

In Eq. (31), $U_{3b}^{(2)}(R_{IJ})$ is the pairwise contribution from the three-body force-matching, and $U^{(3)}(\theta_{JIK}, R_{IJ}, R_{IK})$ is the three-body interaction from Eq. (30). The latter term is projected onto the pairwise basis sets using the bottom-up conditional probability $p(\theta_{JIK}, R_{IK}|R_{IJ})$ and the coordination number at the first coordination shell N_c. We will illustrate the physical principles of the force-matching methodology in Subsection II D 2. From Eq. (31), we demonstrated that the BUMPer model could faithfully recapitulate the structural correlations of water, such as two-, three-, and multi-body correlations, while retaining pairwise basis sets at an inexpensive computational cost.[143,144] Thus, we envisage that the excess entropy scaling relationship will still hold in the CG water system while recapitulating the structural correlations in water. Readers are referred to Refs. 143 and 144 for the BUMPer theory and detailed discussion.

2. CG methanol model

The CG model for methanol is generated by mapping the methanol molecule to the center-of-mass at a single-site level. Then, the CG interaction parameters between the methanol CG sites are parameterized by the MS-CG method.[150–154] In a practical sense, the force-matching technique was employed by matching the mapped FG forces exerted on the center-of-mass $\mathbf{f}_I(\mathbf{R}^N)$ to the CG force $\mathbf{F}_I(\boldsymbol{R}^N)$. This is variationally determined by minimizing the force residual functional $\chi^2[\mathbf{F}]$ defined as

$$\chi^2[\mathbf{F}] = \frac{1}{3N}\left\langle \sum_{I=1}^{N} \left|\mathbf{f}_I(\mathbf{R}^N) - \mathbf{F}_I(M_{\mathbf{R}}^N(\mathbf{r}^n))\right|^2 \right\rangle, \quad (32)$$

where $\mathbf{r}^n$ and $\mathbf{R}^N$ denote FG and CG configurational variables linked by the mapping operator $M_{\mathbf{R}}^N : \mathbf{r}^n \to \mathbf{R}^N$. Here, $\mathbf{f}_I(\mathbf{R}^N)$ denotes the microscopic force acting on the set $\mathcal{I}_I$ of FG particles i that are mapped into the CG particle I via $M_{\mathbf{R}}^N$, i.e., $\mathbf{f}_I(\mathbf{R}^N) = \sum_{i\in\mathcal{I}_I} \mathbf{f}_i(\mathbf{r}^n)$. Specifically, CG methanol force fields are also spanned over pairwise basis sets $\{\phi_2\}$ as in the CG water force fields. Unlike water, it has been shown that the pairwise representation of methanol interactions can sufficiently capture the structural correlations at a renormalized CG resolution.[150,153,155] Hence, the many-body projection theory accompanied by BUMPer is not needed for methanol. Instead, we expand the interaction by adopting pairwise decomposition as follows:

$$\mathbf{F}_I(M_{\mathbf{R}}^N(\mathbf{r}^n)) = \boldsymbol{F}_I(\mathbf{R}^N) = \sum_J \phi_2(R_{IJ}) \cdot \hat{e}_{IJ}. \quad (33)$$

In practice, we utilize B-splines to approximate the pairwise basis sets $\phi_2(R_{IJ}) = \sum_k c_k u_k(R_{IJ})$ with respect to the unit vector $\hat{e}_{IJ}$. Therefore, Eq. (32) imparts the optimized spline coefficients $\{c_k\}$ that minimizes $\chi^2[\mathbf{F}]$.

E. Computational details

All simulations in this work were performed by employing the Large-scale Atomic/Molecular Massively Parallel Simulator (LAMMPS) MD engine.[156–158] The FG and CG systems of water[143,144] and methanol[128] were prepared based on our previous publications. In detail, the water system is composed of 512 molecules, and the methanol system consists of 1000 molecules after the energy-minimization process.

Atomistic force fields were chosen as follows: SPC/E,[159] SPC/Fw,[160] TIP4P/2005,[161] and TIP4P/ice[162] for water and Optimized Potentials for Liquid Simulations/All Atom (OPLS/AA) for methanol.[163,164] The equilibrium system size is chosen from the FG simulations at 300 K and 1 atm condition. This is done by initially annealing the relaxed system using constant *NVT* dynamics with a Nosé–Hoover thermostat[165,166] with $\tau_{\mathrm{NVT}} = 0.1$ ps for 0.1 ns, followed by constant *NPT* dynamics for 1 ns using the Andersen barostat.[167] At the target temperature, we generated the FG trajectories for 5 ns under constant *NVT* dynamics using the same settings.

From the *NVT* trajectories, the effective CG interactions of BUMPer were parameterized based on Refs. 143 and 144. For methanol, Eq. (33) was implemented by employing the sixth order B-splines with a resolution of 0.20 Å. The obtained inner-core interactions were additionally fitted to the $A \cdot \mathbf{R}^{-B}$ form to account for a poor sampling in the core area.[168] Using the parameterized CG interactions, we ran the CG simulations for analysis under a constant *NVT* ensemble with a Nosé–Hoover thermostat[165,166]

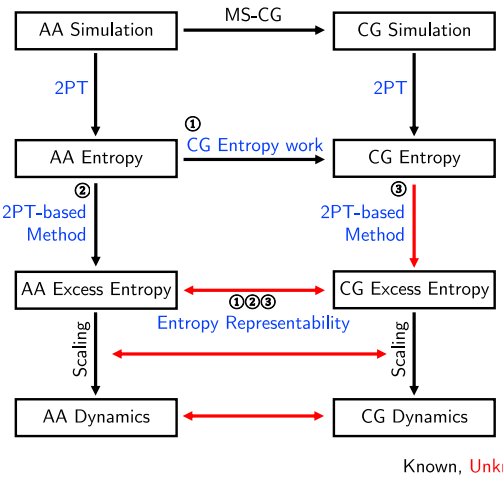

FIG. 1. Schematic diagram describing the correspondence between the FG and CG dynamics. Dynamical properties are obtained by excess entropy scaling, which is determined by system entropy using the 2PT-based method in this work (blue). Our work aims to understand the unknown links (red) to provide a comprehensive understanding of FG and underlying CG dynamics.

for 5 ns. For both FG and CG simulations, we collected the configurations every 1 ps.

In summary, Fig. 1 shows the schematic flowchart of this paper. From the FG (atomistic) simulations, we can calculate the overall entropy and then excess entropy. Applying the Rosenfeld scaling to the excess entropy, we can link this excess entropy to the dynamical information. While the same logic applies to the CG system, in this section, we introduced a new method to calculate the excess entropy ② and revisited the entropy representability relationship between the FG and CG counterparts ① and ③. The remainder of this paper will be devoted to examining the suggested theory and methodology.

III. RESULTS AND DISCUSSIONS

A. CG model interaction

Parameterized CG models are shown in Fig. 2. Since the excess entropy is a function of (number) density and temperature, $S_{ex} = S_{ex}(\rho, T)$, we fixed the volume from the $T = 300$ K and $P = 1$ atm condition while changing temperature to obtain different S_{ex} values. The main reason for fixing the volume is to enforce the constant volume condition for parameterizing the CG interactions. Since bottom-up CG models identify the many-body CG PMF as the CG interaction, the effective CG interaction should also be interpreted as a free energy quantity.[152] In order to consider the changes in CG PMFs at different temperatures, the CG PMFs were designed to be temperature transferable under constant volume, where the pairwise free energy functional can be interpreted as the Helmholtz free energy ($\Delta F = \Delta E - T\Delta S$): $U_{CG}(R) = \Delta E(R) - T\Delta S(R)$,[128,169,170] where $\Delta E(R)$ and $\Delta S(R)$ denote the pair energy and entropy functional, respectively. In Refs 10, 128, and 155, this notational choice was discussed in detail. In addition, due to the energy representability, $\langle \Delta E(R) \rangle_{CG}$ corresponds to the average energy of the FG system, i.e., $\langle U_{FG}(\mathbf{r}^n) \rangle_{FG}$.[171,172]

Previously, we have demonstrated that the changes in CG PMFs over temperature, characterized as $\Delta U_{CG}(R)/\Delta T$, remain constant across different temperature ranges (280–360 K for water[143,144] and 250–400 K for methanol[128,155]), confirming the temperature transferability of CG models. This linear nature of the temperature-dependent nature of CG interactions is plotted in Fig. 2. Moreover, we observe that both liquid CG interactions have double-well interactions. However, in the CG water models, we note a clear separation between two wells with a repulsive barrier near 3.3 Å, suggesting the strongly structured pair correlations compared to liquid methanol. We point the reader to a comprehensive overview and analysis of the BUMPer CG interactions in Refs. 143 and 144.

B. Diffusion in FG/CG models

From the FG simulations and corresponding CG trajectories at different temperatures, we computed the self-diffusion coefficients for water and methanol. The molecular self-diffusion coefficients

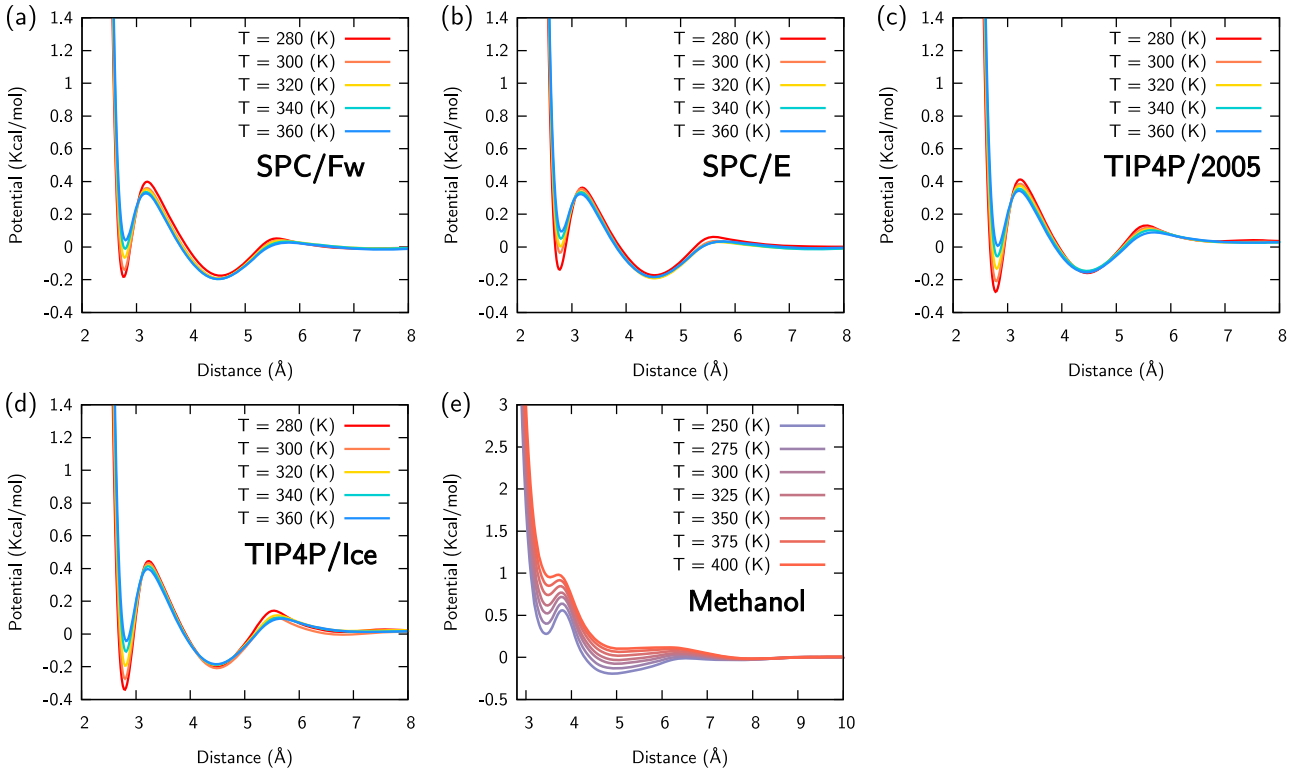

FIG. 2. Temperature-dependent effective CG pair interactions for the CG model of (a)–(d) water and (e) methanol. For water, different BUMPer models were constructed based on the atomistic force field: (a) SPC/E, (b) SPC/Fw, (c) TIP4P/2005, and (d) TIP4P/ice with different temperatures ranging from 280 K (red) to 360 K (blue). CG methanol models are also constructed for different temperatures from 250 K (blue) to 400 K (red).

were readily calculated from the center-of-mass mean squared displacement (MSD),

$$\left\langle R^2(t)\right\rangle := \left\langle \left|\vec{R}(t) - \vec{R}_0\right|^2 \right\rangle = \frac{1}{N}\sum_{I}^{N} \left|\vec{R}_I(t) - \vec{R}_I(0)\right|^2. \quad (34)$$

Thus, from Einstein's relation, we arrive at the diffusion coefficient given as

$$D = \lim_{t\to\infty} \frac{1}{6t}\left\langle R^2(t)\right\rangle. \quad (35)$$

We also alternatively calculated D from the Green–Kubo (GK) formalism using the VACF $C_{vv}(t)$,[173]

$$D = \frac{1}{3}\int_0^\infty C_{vv}(t)dt = \frac{1}{3}\int_0^\infty \langle \vec{v}(t)\cdot\vec{v}(0)\rangle dt. \quad (36)$$

Determination of $C_{vv}(t)$ and the GK calculation were performed in the 2PT program suite, where the velocity autocorrelation was computed by averaging the x-, y-, and z-components of velocity due to isotropy. Even though both approaches give similar values, GK diffusion coefficients are relatively larger and less converged due to the convergence issues of the VACF as reported in the 2PT benchmark paper.[120] Based on this finding, we herein report the diffusion coefficients computed from the MSD.

Figure 3 shows the calculated diffusion coefficients of water and methanol for different FG and CG models at various temperature ranges. We used a range between 280–360 K for water and 250–400 K for methanol. The trend of the diffusion coefficients indicates that the temperature ranges studied here fall into the normal liquid regime. For both molecular systems, we observe that the FG diffusivity increases with the temperature as expected, and this trend is also seen in the CG force fields. For water, this trend is invariant under different choices of FG force fields as well. However, we note that the FG diffusion coefficients among the four FG models are slightly different. Even though this mismatch stands out in the case of TIP4P/ice, this can be understood from the fact that TIP4P/ice (unlike the SPC/E model) was designed to match the melting point of the ice, not dynamical properties.[162]

As discussed earlier, the CG dynamics in the Hamiltonian system are generally significantly faster than the FG dynamics, and this acceleration factor is quantified as D_{CG}/D_{FG}. Figure 3(a) indicates that D_{CG}/D_{FG} of water monotonically decreases as the temperature increases from 280 to 360 K. Roughly speaking, D_{CG}/D_{FG} falls from a factor of 8–12 at 280 K to 3–4 at 360 K. This trend seems consistent regardless of the FG force fields, indicating an Arrhenius-like behavior of the diffusion coefficient for both water and methanol.

In order to perform excess entropy scaling, we rescaled the diffusion coefficient using the elementary or macroscopic units shown in Eq. (3). Since the CG models and dynamical properties are obtained under the constant volume condition, the size of the simulation box was fixed as $L_{H_2O} = 25.022$ Å for water according to the original paper with $N = 512$.[143,144] With these conditions, we arrive at the reduced diffusion coefficient of water as a function of temperature as

$$D^* = D\frac{\rho^{\frac{1}{3}}}{(k_BT/m)^{\frac{1}{2}}} = 1.4880\times10^4 \times \frac{D}{\sqrt{T}}. \quad (37)$$

For methanol, the reduced diffusion coefficient was similarly scaled by the following equation with $N = 1000$ and $L_{MeOH} = 41.30$ Å:

$$D^* = D\frac{\rho^{\frac{1}{3}}}{(k_BT/m)^{\frac{1}{2}}} = 1.5029\times10^4 \times \frac{D}{\sqrt{T}}. \quad (38)$$

Table I lists the reduced diffusion coefficients for both FG and CG models at different temperatures.

C. Excess entropy scaling: Water

We next utilized the theory described here to calculate the excess entropy and then examine the validity of the Rosenfeld scaling for various state points of water. First, the translational entropy

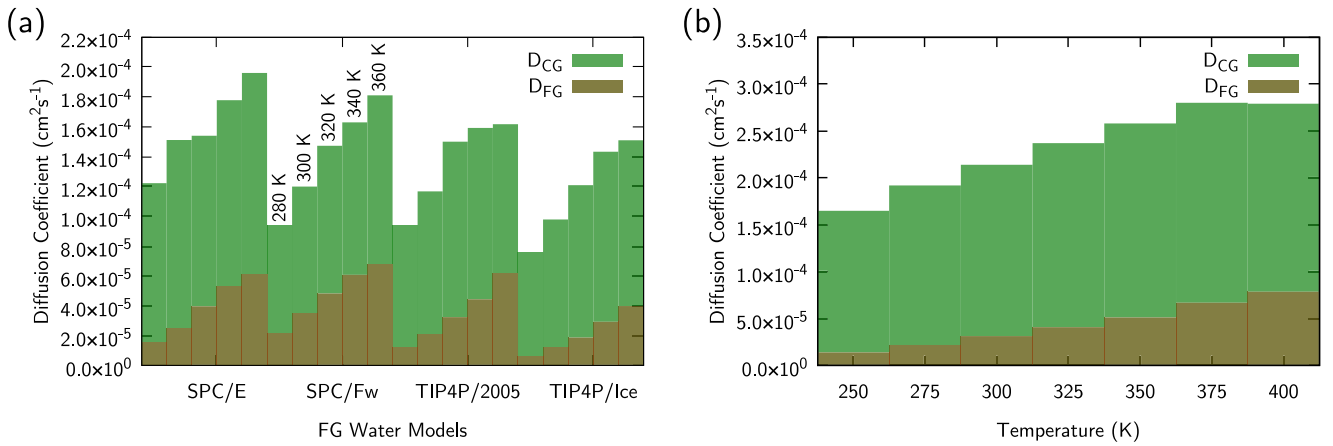

FIG. 3. Diffusion coefficients of water and methanol evaluated for FG (brown bars) and CG (green bars) systems at different temperatures in each column. (a) Water: SPC/E, SPC/Fw, TIP4P/2005, and TIP4P/ice force fields from 280 to 360 K at 20 K intervals. (b) Methanol: OPLS-AA force field at a temperature range from 250 to 400 K at 25 K intervals.

TABLE I. Macroscopically reduced diffusion coefficients of the water and methanol systems at the FG (D^*_{FG}) and CG (D^*_{CG}) resolutions. For water, we scanned the temperature from 280 to 360 K using four FG force fields and corresponding BUMPer CG models: (a) SPC/E, (b) SPC/Fw, (c) TIP4P/2005, and (d) TIP4P/ice. For methanol (e), we used a temperature ranging from 250 to 400 K using OPLS-AA force fields and the corresponding MS-CG model.

Temperature (K)	D^*_{FG}	D^*_{CG}	Temperature (K)	D^*_{FG}	D^*_{CG}
(a) SPC/E: Water			(b) SPC/Fw: Water		
280	1.379×10^{-2}	1.087×10^{-1}	280	1.955×10^{-2}	8.349×10^{-2}
300	2.152×10^{-2}	1.298×10^{-1}	300	3.031×10^{-2}	1.030×10^{-1}
320	3.310×10^{-2}	1.280×10^{-1}	320	4.022×10^{-2}	1.225×10^{-1}
340	4.305×10^{-2}	1.434×10^{-1}	340	4.910×10^{-2}	1.314×10^{-1}
360	4.797×10^{-2}	1.537×10^{-1}	360	5.312×10^{-2}	1.419×10^{-1}
(c) TIP4P/2005: Water			(d) TIP4P/ice: Water		
280	1.070×10^{-2}	8.368×10^{-2}	280	5.370×10^{-3}	6.757×10^{-2}
300	1.812×10^{-2}	1.003×10^{-1}	300	1.068×10^{-2}	8.411×10^{-2}
320	2.705×10^{-2}	1.247×10^{-1}	320	1.567×10^{-2}	1.005×10^{-1}
340	3.590×10^{-2}	1.284×10^{-1}	340	2.375×10^{-2}	1.156×10^{-1}
360	4.864×10^{-2}	1.268×10^{-1}	360	3.134×10^{-2}	1.183×10^{-1}
(e) OPLS-AA: Methanol					
250	1.354×10^{-2}	1.566×10^{-1}	350	4.131×10^{-2}	2.073×10^{-1}
275	2.005×10^{-2}	1.736×10^{-1}	375	5.207×10^{-2}	2.174×10^{-1}
300	2.743×10^{-2}	1.859×10^{-1}	400	5.924×10^{-2}	2.095×10^{-1}
325	3.427×10^{-2}	1.980×10^{-1}			

of the FG system in an ideal gas description was calculated using the following constants: $N = 512$, $m_w = 18.015 \times 10^{-3}$ kg, and $L_{H_2O} = 25.022$ Å, giving

$$s^{(id)}_{trn} = -\ln\left[\frac{\left(6.6262 \times 10^{-34}\mathrm{m^2\,kg\,s^{-1}}\right)^2}{2\pi\left(\frac{18.015\times10^{-3}\mathrm{kg}}{6.02214\times10^{23}}\right) \times 1.381 \times 10^{-23}\mathrm{J\,K^{-1}} \times T}\right]^{\frac{3}{2}} - \ln\left[\frac{512}{\left(25.022 \times 10^{-10}\mathrm{m}\right)^3}\right] + \frac{5}{2} = 1.6787 + \frac{3}{2}\ln T. \quad (39)$$

As expected, the final result of Eq. (39) shows that the ideal gas entropy is only a function of temperature and number density. Next, we utilized Eq. (24) to calculate the rotational excess entropy of water. From the characteristic rotational temperatures $\Theta_A = 40.1$, $\Theta_B = 20.9, \Theta_C = 13.4$ K and the C_{2v} symmetry ($\sigma = 2$), we arrive at the following expression:

$$s^{(id)}_{rot} = -3.2840 + \frac{3}{2}\ln T. \quad (40)$$

Combining Eqs. (39) and (40), the final analytical expression is written as

$$s^{FG}_{ex} = S^{FG} - \left(-3.2840 + \frac{3}{2}\ln T\right) - \left(1.6787 + \frac{3}{2}\ln T\right). \quad (41)$$

Figure 4(a) plots s^{FG}_{ex} over $\ln D^*_{FG}$ for different FG force fields. Before examining the scaling behavior, we first verified that the 2PT method provides physically reasonable excess entropy values. In other words, for all the data points shown in Fig. 4(a), we confirmed that $s^{ex}_{trn}|_{FG} = s^{FG}_{trn} - s^{(id)}_{trn} < 0$ and $s^{ex}_{rot}|_{FG} = s^{FG}_{rot} - s^{(id)}_{rot} < 0$, suggesting a well-defined excess entropy.

It is immediately evident that the linear scaling relationship is satisfied in water regardless of the force field or temperature. In particular, this scaling relationship is given by

$$\ln D^*_{FG} = 0.73 \times s^{FG}_{ex} + 2.15. \quad (42)$$

We note that this exponent is slightly different from the original exponent from Rosenfeld because the original Rosenfeld scaling was computed for the translational component of the system, lacking configurational effects. We believe that this deviation is due to the contribution from the local configurational ordering of water, especially rotational motions.

In order to verify the universality of the scaling relationship between FG and CG systems, we compared s^{CG}_{ex} over $\ln D^*_{CG}$ in Fig. 4(b). This is done by calculating the CG excess entropy from translational contributions,

$$s^{(id)}_{trn}|_{CG} = 1.6787 + \frac{3}{2}\ln T. \quad (43)$$

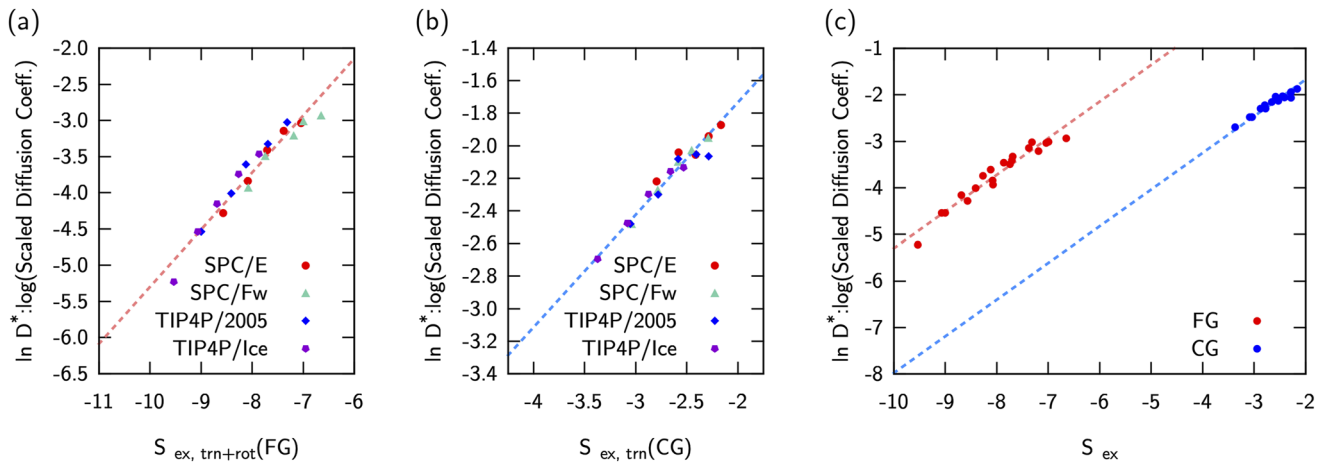

FIG. 4. Examination of the Rosenfeld scaling in water. (a) FG scaling relationship where the SPC/E (red circle), SPC/Fw (green triangle), TIP4P/2005 (blue diamond), TIP4P/ice (purple pentagon) models fall into a linear scaling relation shown in Eq. (42) (red dashed line). (b) CG scaling relationship using the BUMPer CG model by parameterizing different force fields. Similarly, a linear excess entropy relationship is obtained (blue dashed line) from Eq. (43). (c) Overall comparison between the FG (red circle) and CG (blue circle) water models. Note that the slope (exponent) of the FG scaling (red dashed line) is identical to that of the CG scaling relation (blue dashed line), while only the *y*-intercept is different.

As expected, we find that $s^{ex}_{trn}|_{CG} = s^{CG}_{trn} - s^{(id)}_{trn} < 0$ in the CG system as well. Surprisingly, we still see a linear dependency given by the following relation:

$$\ln D^*_{CG} = 0.7 \times s^{CG}_{ex} - 0.35. \tag{44}$$

The exponent α obtained from the FG and CG seems slightly different at first glance. Our finding here shows different results with respect to the previous work for the diffusion of the FG and CG water systems.[78] In this previous effort, the authors used the Dzgutov scaling [Eq. (4)] instead of the Rosenfeld scaling [Eq. (2)] to obtain a dimensionless diffusion coefficient. As discussed earlier, Eq. (4) was primarily derived for hard sphere diffusion processes only using pairwise entropy information, which does not hold for water due to hydrogen bonding and large contribution beyond pairwise contributions. In addition, while Ref. 78 aimed to compute the orientational entropy based on Refs. 108–112, the computed orientational entropy by sampling various angular configurations may pose a convergence issue.[116,117] We believe that these factors in Ref. 78 result in different scaling exponents for FG and CG water, $\alpha^{FG} = 0.594$ and $\alpha^{CG} = 2.373$, which significantly deviate from the conventional Rosenfeld scaling relationship. More importantly, an overestimated CG exponent value of about eight times indicates that the accurate estimation of excess entropy with a correct scaling scheme is necessary for CG systems. By including all contributions to the entropy with a more accurate scaling relationship as done here, we instead conclude that both FG and CG systems have almost identical scaling relationships, where both exponents also correspond to the range of conventional Rosenfeld scaling. This trend is pronounced in Fig. 4(c), where both FG and CG data points follow nearly identical slopes.

At this point, a natural question arises in terms of differences in $\ln D^*$. As envisaged, the CG system has a larger excess entropy (closer to zero) because the CG system does not have rotational excess entropy. Note that excess entropy is always less than zero, and thus, having a less negative value contributes to near positive values (the differences between these entropies will be discussed in Sec. III E). Indeed, it would be of great interest if this agreement between $\alpha^{FG} = \alpha^{CG}$ still holds in other molecular systems to confirm a general correspondence.

D. Methanol

Given the same scaling behavior obtained in the FG and CG water systems, we now examine the excess entropy scaling of methanol. For the atomistic (FG) methanol, both translational and rotational degrees of freedom contribute to the entropy (vibrational modes are negligible). Using the Sackur–Tetrode equation, the translational entropy of the ideal gas corresponding to the center-of-mass is given as

$$s^{(id)}_{trn} = -\ln\left[\frac{\left(6.6262\times10^{-34}\text{m}^2\ \text{kg}\ \text{s}^{-1}\right)^2}{2\pi\left(\frac{32.042\times10^{-3}\text{kg}}{6.02214\times10^{23}}\right)\times 1.381\times10^{-23}\text{J}\ \text{K}^{-1}\times T}\right]^{\frac{3}{2}} - \ln\left[\frac{1000}{\left(41.30\times10^{-10}\text{m}\right)^3}\right] + \frac{5}{2} = 3.3764 + \frac{3}{2}\ln T. \tag{45}$$

The rotational partition function of methanol is relatively difficult to construct since it requires an actual measurement of the molecular data in the mm to sub-mm wavelength regime. Fortunately, we found the experimental observable, giving the rotational frequency $\overline{B} = 4.257\,30$, $0.823\,38$, and $0.792\,73\ \text{cm}^{-1}$.[174] Converting $\overline{B}$ to the characteristic rotational temperatures using

$$\Theta_R = \frac{hc\overline{B}}{k_B} = 1.439\times\overline{B} \tag{46}$$

results in $\Theta_R = 6.125, 1.185$, and 1.140 K. Substituting these Θ_R values in Eq. (24) gives the final expression for the rigid rotor,

$$s_{\rm rot}^{\rm (id)} = -0.08295 + \frac{3}{2}\ln T. \tag{47}$$

Altogether, we finally arrive at the excess entropy expression for methanol,

$$s_{ex}^{\rm FG} = s^{\rm FG} - \left(-0.08295 + \frac{3}{2}\ln T\right) - \left(3.3764 + \frac{3}{2}\ln T\right). \tag{48}$$

Figure 5(a) delineates the scaling relationship in the FG methanol. Remarkably, one obtains a linear relationship in the methanol system as well, given by

$$\ln D^*_{\rm FG} = 0.65 \times s_{ex}^{\rm FG} + 0.62. \tag{49}$$

As discussed above, we note differences in $\alpha^{\rm FG}_{\rm H_2O}$ and $\alpha^{\rm FG}_{\rm MeOH}$ due to different rotational and translational contributions. However, as long as $\alpha^{\rm FG}_{\rm MeOH}$ is close to $\alpha^{\rm CG}_{\rm MeOH}$, our universality hypothesis remains valid.

To assess $\alpha^{\rm CG}_{\rm MeOH}$, we apply a similar procedure to CG methanol by only accounting for the translational degrees of freedom,

$$s_{\rm trn}^{\rm (id)}|_{\rm CG} = \frac{S_{\rm trn}^{\rm (id)}}{Nk_B}|_{\rm CG} = 3.3764 + \frac{3}{2}\ln T. \tag{50}$$

An overall trend observed in the CG systems is illustrated in Fig. 5(b), and a slight discrepancy observed in 400 K can be understood from the atomistic trend depicted in Fig. 3. Nevertheless, we find linearity over a wide range of temperatures from 250 to 400 K in the following form:

$$\ln D^*_{\rm CG} = 0.65 \times s_{ex}^{\rm FG} - 0.84. \tag{51}$$

In other words, we conclude here again $\alpha^{\rm FG}_{\rm MeOH} = \alpha^{\rm CG}_{\rm MeOH}$, as can be seen in Fig. 5(c). The universality of α for methanol was further tested by checking if the same scaling relationship will hold for different resolutions. Based on the two-site CG mapping studied in Ref. 175, a two-site CG methanol model was constructed by mapping CH_3– and OH– atoms to CG sites. In this CG model, the CG excess entropy must consider additional rotational and vibrational motions along the C–O bond, i.e., Eqs. (45)–(48). Interestingly, Fig. 9 in the Appendix clearly demonstrates that two-site CG methanol also follows the nearly identical scaling relationship as the single-site model, confirming our perspective on universality.

To conclude, we have discovered through an analysis of water and methanol that the excess entropy scaling relationship holds for both the FG and CG systems. More importantly, a universality relationship for simple liquids was elucidated for the first time that, given the same molecular system, the exponent (or slope in $\ln D^*$) from the scaling relationship remains invariant during the coarse-graining process. That is, $\alpha^{\rm FG} = \alpha^{\rm CG}$, indicating that the scaling relationship is intrinsically related to the underlying nature of the molecule, and thus, it is still captured in the "bottom-up" CG models. Given the accelerated diffusion coefficient in the CG system, a relevant question is to then explicitly relate the CG diffusion coefficient to its FG analog in the scaled form.

E. Relationship with mapping entropy

From Eqs. (5) and (6), the differences in diffusion coefficient between the FG and CG levels are due to two factors in the scaling relationship: D_0 and S_{ex}. The differences between the $S_{ex}^{\rm FG}$ and $S_{ex}^{\rm CG}$ terms can be clearly understood from the coarse-graining process. Since less important degrees of freedom are integrated out

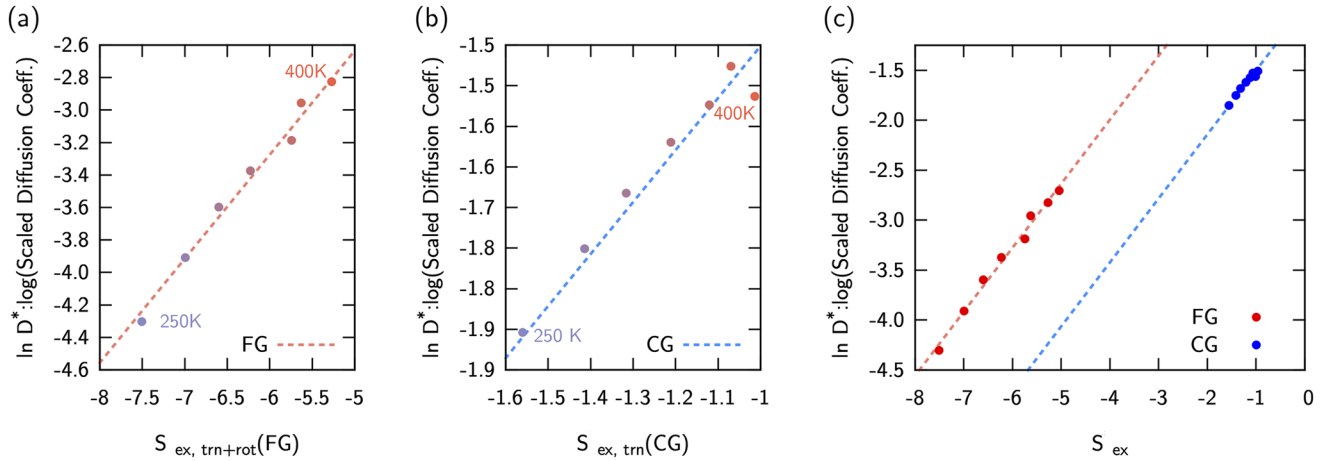

FIG. 5. Examination of the Rosenfeld scaling in methanol. (a) FG scaling relationship over different temperatures from 250 K (bottom, left) to 400 K (top, right) fall into a linear scaling relation shown in Eq. (49) (red dashed line). (b) CG scaling relationship using the CG methanol model. Similarly, a linear excess entropy relationship is obtained (blue dashed line) from Eq. (50). (c) Overall comparison between the FG (red circle) and CG (blue circle) methanol models. Note that the slope (exponent) of the FG scaling (red dashed line) is identical to that of the CG scaling relation (blue dashed line), while only the y-intercept is different.

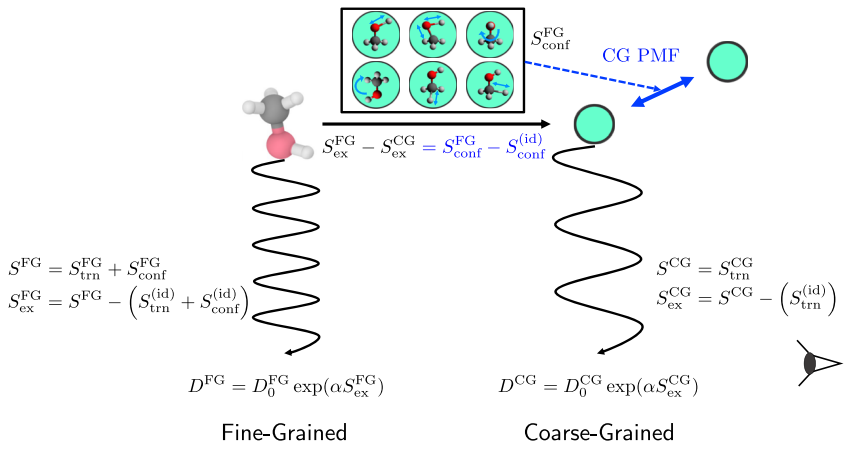

FIG. 6. The present understanding of FG/CG dynamics in terms of excess entropy scaling. With an identical excess entropy scaling confirmed in this work, fast dynamics observed in the CG model can be understood from the mapping entropy $S^{\mathrm{FG}}_{\mathrm{conf}}$ and from different D_0 values.

during the bottom-up coarse-graining process, the configurational entropy of the resultant CG model is reduced compared to the reference configurational entropy at the FG level. As discussed above, for the single-site CG model, this missing entropy, known as "mapping entropy," corresponds to the motions "beneath" the CG resolution: in this case rotation and vibration.[128] Figure 6 summarizes our understanding of the CG excess entropy scaling relationship with respect to the one obtained from the FG model. By decomposing the overall entropy into its underlying modes, it is evident that the motions observed in the CG dynamics are fully from translational motions $S^{\mathrm{CG}} = S^{\mathrm{CG}}_{\mathrm{trn}}$, corresponding to the translational entropy at the FG resolution $S^{\mathrm{CG}}_{\mathrm{trn}}$. In other words, the differences in the excess entropy terms are primarily from the $S^{\mathrm{FG}}_{\mathrm{conf}}$ term, importantly, indicating that one can adjust the CG entropy term with respect to the FG model to rescale the diffusion behavior.

IV. CONCLUSIONS

In this paper, we have elucidated the accelerated dynamical properties in CG fluid systems compared to the reference FG system by introducing an excess entropy scaling. While various studies have focused on the excess entropy in order to understand the FG dynamics, relatively less attention has been given to CG systems. However, based on the observation of missing motions in a given CG model and their corresponding contributions to the excess entropy, we assert that the excess entropy scaling can help to understand the speed-up of the CG dynamics. By combining the 2PT method and taking into consideration the orientational contributions, we were able to propose a comprehensive approach to computing the excess entropy for CG systems and the corresponding FG systems. Unlike other conventional approaches, we utilize the 2PT-based decomposition of molecular motions for the translational, vibrational, and rotational contributions as this method has been shown to quantify the missing entropy during the coarse-graining process. By taking the ideal gas entropy from the Sackur–Tetrode equation for translation and using a rigid rotor entropy for rotation, we derived the excess entropy scaling behavior for both water and methanol at the atomistic (FG) level. By extending this approach to the CG systems, we observed that the same scaling behavior exists with an identical scaling exponent for each molecular system. To our knowledge, this finding corroborates the universality and invariance of the excess entropy scaling under the coarse-graining process for liquid molecules studied in this work. Our finding also substantiates an earlier claim from Ref. 79 that proposed a connection between relative entropy differences and the dynamical behavior of liquids. Furthermore, the present theory proposes an alternative approach to accurately calculate the excess entropy for any molecular system and the corresponding CG model as long as one can construct ideal gas partition functions from known structural parameters. This requires a faithful construction of bottom-up CG models by considering the correct modal contribution to the excess entropy at the given resolution.

Combining these pieces together, the present theory enables one to link the missing (or mapping) entropy with the faster CG dynamics followed by the identical scaling behavior as in the FG model. By correcting the missing entropy to CG systems, introducing the rotational entropies from the FG model would further lower the excess entropy since $S^{(\mathrm{rot})}_{ex} < 0$, resulting in slower CG dynamics. Hence, if the D_0 value for the FG model is known, it is possible to rescale the accelerated CG dynamics to the FG dynamics value by correcting the mapping entropy due to the coarse-graining following the formulation in Ref. 128 and adjusting D^{CG}_0 to D^{FG}_0. We further applied this idea to CG water systems in Fig. 7, where the recovered FG diffusion coefficients from CG dynamics $D^{\mathrm{corr}}_{\mathrm{CG}}$ show almost identical values as the original FG diffusion with an error of 4.5% for SPC/E, 2.1% for SPC/Fw, 5.7% for TIP4P/2005, and 2.4% for TIP4P/ice. We note that a similar approach was recently suggested by Rondina *et al.* for rescaling dynamics at different CG resolutions of Lennard-Jones chains of polymers using the Dzugutov scaling.[80]

Nevertheless, for complex molecules governed by the Rosenfeld scaling, the *ad hoc* nature of D_0 and alpha values are a current bottleneck to bridge dynamics between the FG and CG dynamics. To elaborate more on this viewpoint, Fig. 8 demonstrates that the corrected CG diffusion coefficient and reference FG diffusion coefficient simply based on the excess entropy differences do not completely agree with each other due to the difference in the D_0 terms. Despite having the same scaling exponent, we see differences

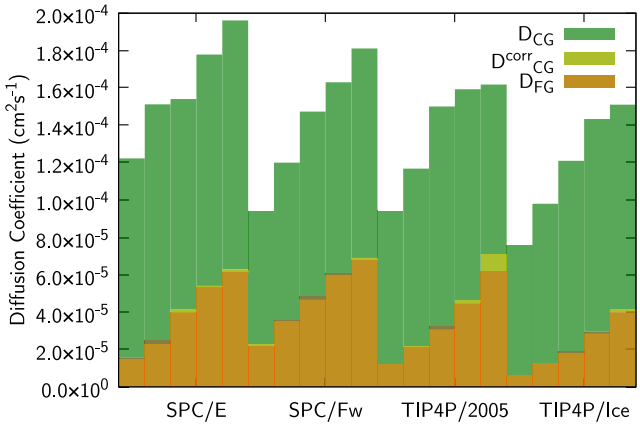

FIG. 7. Corrected diffusion coefficients of water (yellow bars) from CG (green bars), given the FG scaling intercept D_0^{FG}. Note that the rescaled CG diffusion coefficients can reproduce the original FG diffusion coefficients (orange bars). Four force fields from 280 to 360 K at 20 K intervals are considered.

in the D_0 values (which we think of as an "entropy-free" diffusion coefficient) between the FG and CG models. Thus, a better understanding of the physical meaning and origin of the D_0 term, as well as their excess entropy difference, is required.

Nevertheless, the phenomenological foundations of the scaling behavior limit further theoretical analysis of the D_0 term for both the FG and CG systems. Even though the FG dynamics involve complicated coupled motions with different time scales, the single-site CG resolution can integrate these extraneous motions out, leaving the translational motions only. Thus, in order to systematically better understand the meaning of D_0 and to develop approaches for its calculation, it may be physically sound to approximate the reduced CG dynamics as hard sphere dynamics. This approach is pursued further in Paper II of this series with the goal of providing a more complete description of the CG model diffusion based on the universal scaling law between the CG and FG systems of fluids as uncovered in this paper.[176]

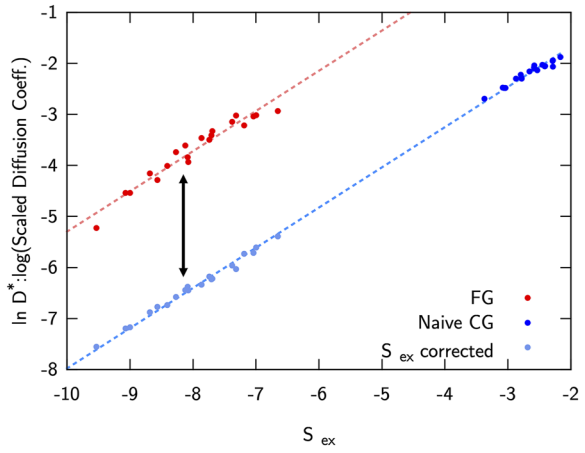

FIG. 8. Excess entropy scaling (dashed lines) of water for FG (red dots) and CG systems (blue dots) and after adjusting the mapping entropy to the CG model (sky blue dots).

ACKNOWLEDGMENTS

This work was supported by the National Science Foundation (NSF, Grant No. CHE-2102677). Simulations were performed using computing resources provided by the University of Chicago Research Computing Center (RCC). J.J. acknowledges the Harper Dissertation Fellowship from the University of Chicago and insightful discussions with Professor Jeppe C. Dyre. K.S.S. acknowledges the support of the University of Chicago and the Pritzker School of Molecular Engineering during his sabbatical stay where this work was initiated.

AUTHOR DECLARATIONS

Conflict of Interest

The authors have no conflicts to disclose.

Author Contributions

Jaehyeok Jin: Conceptualization (equal); Formal analysis (equal); Investigation (equal); Methodology (equal); Software (equal); Validation (equal); Visualization (equal); Writing – original draft (equal); Writing – review & editing (equal). **Kenneth S. Schweizer**: Conceptualization (equal); Investigation (equal); Supervision (equal); Validation (equal); Writing – review & editing (equal). **Gregory A. Voth**: Conceptualization (equal); Funding acquisition (equal); Investigation (equal); Project administration (equal); Resources (equal); Supervision (equal); Validation (equal); Writing – review & editing (equal).

DATA AVAILABILITY

The data that support the findings of this study are available from the corresponding author upon reasonable request.

APPENDIX: TWO-SITE CG METHANOL MODEL

The two-site CG model for methanol was constructed by following the same procedures described in Ref. 175. First, the CG sites were determined by mapping CH_3– and OH– atoms to the center-of-mass of each group. Parameterization settings for nonbonded interactions were kept identical to the single-site case, while the bonded interaction was described by the fourth order B-splines with smaller spacing (0.025 Å). After parameterizing the two-site CG methanol model from MS-CG, the same simulation protocol was used to run CG simulations at different temperatures as in Fig. 5. The excess entropy scaling was accessed by computing the additional rotational and vibrational motions remained at the two-site CG level. In Fig. 9, we observe that the fitted slope of the two-site CG model differs by a value of 0.009 compared to the single-site CG scaling relationship. Hence, we believe that the two-site CG model also follows the nearly identical scaling exponent as the single-site CG model, indicating that the scaling relationship is invariant for methanol under different resolutions.

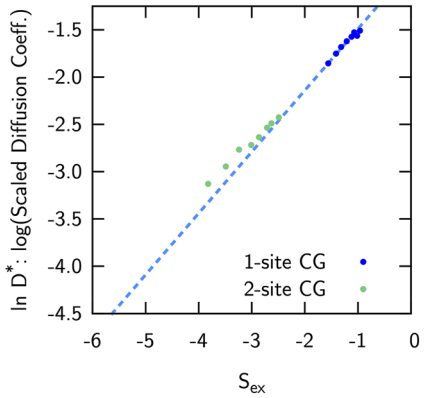

FIG. 9. Rosenfeld scaling for CG methanol at different resolutions. Results from the one-site CG model (blue circles) and a linear relationship from Fig. 5 (blue dashed line) were directly on top of the results from the two-site CG model (green circle). Differences between the fitted slopes and *y*-intercept for two CG resolutions are obtained as 0.009 and 0.03, respectively, and are deemed negligible.

REFERENCES

[1] F. Müller-Plathe, ChemPhysChem **3**(9), 754–769 (2002).
[2] H. A. Scheraga, M. Khalili, and A. Liwo, Annu. Rev. Phys. Chem. **58**, 57–83 (2007).
[3] G. A. Voth, *Coarse-graining of Condensed Phase and Biomolecular Systems* (CRC Press, 2008).
[4] C. Peter and K. Kremer, Soft Matter **5**(22), 4357–4366 (2009).
[5] T. Murtola, A. Bunker, I. Vattulainen, M. Deserno, and M. Karttunen, Phys. Chem. Chem. Phys. **11**(12), 1869–1892 (2009).
[6] S. Riniker and W. F. van Gunsteren, J. Chem. Phys. **134**(8), 084110 (2011).
[7] W. G. Noid, J. Chem. Phys. **139**(9), 090901 (2013).
[8] M. G. Saunders and G. A. Voth, Annu. Rev. Biophys. **42**, 73–93 (2013).
[9] A. J. Pak and G. A. Voth, Curr. Opin. Struct. Biol. **52**, 119–126 (2018).
[10] J. Jin, A. J. Pak, A. E. P. Durumeric, T. D. Loose, and G. A. Voth, J. Chem. Theory Comput. **18**(10), 5759–5791 (2022).
[11] J. M. A. Grime and G. A. Voth, Biophys. J. **103**(8), 1774–1783 (2012).
[12] J. M. A. Grime, J. F. Dama, B. K. Ganser-Pornillos, C. L. Woodward, G. J. Jensen, M. Yeager, and G. A. Voth, Nat. Commun. **7**(1), 11568 (2016).
[13] A. J. Pak, J. M. A. Grime, P. Sengupta, A. K. Chen, A. E. P. Durumeric, A. Srivastava, M. Yeager, J. A. G. Briggs, J. Lippincott-Schwartz, and G. A. Voth, Proc. Natl. Acad. Sci. U. S. A. **114**(47), E10056–E10065 (2017).
[14] A. J. Pak, J. M. A. Grime, A. Yu, and G. A. Voth, J. Am. Chem. Soc. **141**(26), 10214–10224 (2019).
[15] A. Yu, K. A. Skorupka, A. J. Pak, B. K. Ganser-Pornillos, O. Pornillos, and G. A. Voth, Nat. Commun. **11**(1), 1307 (2020).
[16] W. Xia, J. Song, C. Jeong, D. D. Hsu, F. R. Phelan, Jr., J. F. Douglas, and S. Keten, Macromolecules **50**(21), 8787–8796 (2017).
[17] W. Xia, J. Song, N. K. Hansoge, F. R. Phelan, Jr., S. Keten, and J. F. Douglas, J. Phys. Chem. B **122**(6), 2040–2045 (2018).
[18] W. Xia, N. K. Hansoge, W.-S. Xu, F. R. Phelan, Jr., S. Keten, and J. F. Douglas, Sci. Adv. **5**(4), eaav4683 (2019).
[19] M. Dunbar and S. Keten, Macromolecules **53**(21), 9397–9405 (2020).
[20] A. Giuntoli, N. K. Hansoge, A. van Beek, Z. Meng, W. Chen, and S. Keten, npj Comput. Mater. **7**(1), 168 (2021).
[21] W. Tschöp, K. Kremer, J. Batoulis, T. Bürger, and O. Hahn, Acta Polym. **49**(2–3), 61–74 (1998).
[22] S. Izvekov and G. A. Voth, J. Chem. Phys. **125**, 151101 (2006).
[23] C. Hijón, P. Español, E. Vanden-Eijnden, and R. Delgado-Buscalioni, Faraday Discuss. **144**, 301–322 (2010).
[24] D. Fritz, K. Koschke, V. A. Harmandaris, N. F. A. van der Vegt, and K. Kremer, Phys. Chem. Chem. Phys. **13**(22), 10412–10420 (2011).
[25] Z. Li, X. Bian, X. Li, and G. E. Karniadakis, J. Chem. Phys. **143**(24), 243128 (2015).
[26] Z. Li, H. S. Lee, E. Darve, and G. E. Karniadakis, J. Chem. Phys. **146**(1), 014104 (2017).
[27] R. Zwanzig, J. Chem. Phys. **33**(5), 1338–1341 (1960).
[28] R. Zwanzig, Phys. Rev. **124**(4), 983 (1961).
[29] R. Zwanzig, Physica **30**(6), 1109–1123 (1964).
[30] H. Mori, Prog. Theor. Phys. **33**(3), 423–455 (1965).
[31] P. Stinis, Proc. R. Soc. London, Ser. A **471**(2176), 20140446 (2015).
[32] T. Kinjo and S.-a. Hyodo, Phys. Rev. E **75**(5), 051109 (2007).
[33] H. Lei, B. Caswell, and G. E. Karniadakis, Phys. Rev. E **81**(2), 026704 (2010).
[34] L. Gao and W. Fang, J. Chem. Phys. **135**(18), 184101 (2011).
[35] S. Izvekov, J. Chem. Phys. **138**(13), 134106 (2013).
[36] Y. Yoshimoto, I. Kinefuchi, T. Mima, A. Fukushima, T. Tokumasu, and S. Takagi, Phys. Rev. E **88**(4), 043305 (2013).
[37] Z. Li, X. Bian, B. Caswell, and G. E. Karniadakis, Soft Matter **10**(43), 8659–8672 (2014).
[38] A. Davtyan, J. F. Dama, G. A. Voth, and H. C. Andersen, J. Chem. Phys. **142**(15), 154104 (2015).
[39] A. Davtyan, G. A. Voth, and H. C. Andersen, J. Chem. Phys. **145**(22), 224107 (2016).
[40] H. Lei, X. Yang, Z. Li, and G. E. Karniadakis, J. Comput. Phys. **330**, 571–593 (2017).
[41] S. Izvekov, J. Chem. Phys. **146**(12), 124109 (2017).
[42] S. Izvekov, Phys. Rev. E **95**(1), 013303 (2017).
[43] G. Jung, M. Hanke, and F. Schmid, J. Chem. Theory Comput. **13**(6), 2481–2488 (2017).
[44] G. Jung, M. Hanke, and F. Schmid, Soft Matter **14**(46), 9368–9382 (2018).
[45] N. Bockius, J. Shea, G. Jung, F. Schmid, and M. Hanke, J. Phys.: Condens. Matter **33**(21), 214003 (2021).
[46] F. Glatzel and T. Schilling, Europhys. Lett. **136**(3), 36001 (2021).
[47] Y. Han, J. Jin, and G. A. Voth, J. Chem. Phys. **154**(8), 084122 (2021).
[48] V. A. Harmandaris and K. Kremer, Soft Matter **5**(20), 3920–3926 (2009).
[49] V. A. Harmandaris and K. Kremer, Macromolecules **42**(3), 791–802 (2009).
[50] K. M. Salerno, A. Agrawal, D. Perahia, and G. S. Grest, Phys. Rev. Lett. **116**(5), 058302 (2016).
[51] I. Y. Lyubimov, J. McCarty, A. Clark, and M. G. Guenza, J. Chem. Phys. **132**(22), 224903 (2010).
[52] I. Lyubimov and M. G. Guenza, Phys. Rev. E **84**(3), 031801 (2011).
[53] I. Y. Lyubimov and M. G. Guenza, J. Chem. Phys. **138**(12), 12A546 (2013).
[54] J. McCarty, A. J. Clark, J. Copperman, and M. G. Guenza, J. Chem. Phys. **140**(20), 204913 (2014).
[55] J. F. Rudzinski, Computation **7**(3), 42 (2019).
[56] V. Klippenstein, M. Tripathy, G. Jung, F. Schmid, and N. F. A. van der Vegt, J. Phys. Chem. B **125**, 4931–4954 (2021).
[57] Y. Rosenfeld, Phys. Rev. A **15**(6), 2545 (1977).
[58] Y. Rosenfeld, Chem. Phys. Lett. **48**(3), 467–468 (1977).
[59] Y. Rosenfeld, J. Phys.: Condens. Matter **11**(28), 5415 (1999).
[60] M. Dzugutov, Nature **381**(6578), 137–139 (1996).
[61] S. Acharya and B. Bagchi, J. Chem. Phys. **153**, 184701 (2020).
[62] L. E. Reichl, *A Modern Course in Statistical Physics* (Wiley VCH, 2016).
[63] J. C. Dyre, J. Chem. Phys. **149**(21), 210901 (2018).
[64] G. Li, C. Liu, and Z. Zhu, J. Non-Cryst. Solids **351**(10–11), 946–950 (2005).
[65] N. Jakse and A. Pasturel, Sci. Rep. **6**, 20689 (2016).
[66] M. Malvaldi and C. Chiappe, J. Chem. Phys. **132**(24), 244502 (2010).
[67] E. Voyiatzis, F. Müller-Plathe, and M. C. Böhm, Macromolecules **46**(21), 8710–8723 (2013).
[68] J. Mittal, J. R. Errington, and T. M. Truskett, Phys. Rev. Lett. **96**(17), 177804 (2006).
[69] J. Mittal, J. R. Errington, and T. M. Truskett, J. Phys. Chem. B **111**(34), 10054–10063 (2007).

[70]W. Götze, *Complex Dynamics of Glass-Forming Liquids: A Mode-Coupling Theory* (Oxford University Press, 2008).
[71]D. R. Reichman and P. Charbonneau, J. Stat. Mech.: Theory Exp. **2005**(05), P05013.
[72]A. Samanta, S. M. Ali, and S. K. Ghosh, Phys. Rev. Lett. **87**(24), 245901 (2001).
[73]A. Samanta, S. M. Ali, and S. K. Ghosh, Phys. Rev. Lett. **92**(14), 145901 (2004).
[74]M. K. Nandi, A. Banerjee, S. Sengupta, S. Sastry, and S. M. Bhattacharyya, J. Chem. Phys. **143**(17), 174504 (2015).
[75]M. Dzugutov, E. Aurell, and A. Vulpiani, Phys. Rev. Lett. **81**(9), 1762 (1998).
[76]H. Pang, Y.-h. Shin, D. Ihm, E. K. Lee, and O. Kum, Phys. Rev. E **62**(5), 6516 (2000).
[77]S. Bastea, Phys. Rev. Lett. **93**(19), 199603 (2004).
[78]J. A. Armstrong, C. Chakravarty, and P. Ballone, J. Chem. Phys. **136**(12), 124503 (2012).
[79]M. S. Shell, J. Chem. Phys. **137**(8), 084503 (2012).
[80]G. G. Rondina, M. C. Böhm, and F. Müller-Plathe, J. Chem. Theory Comput. **16**(3), 1431–1447 (2020).
[81]M. P. Bernhardt, M. Dallavalle, and N. F. A. Van der Vegt, Soft Mater **18**(2–3), 274 (2020).
[82]M. Dzugutov, Phys. Rev. E **65**(3), 032501 (2002).
[83]R. V. Vaz, A. L. Magalhães, D. L. A. Fernandes, and C. M. Silva, Chem. Eng. Sci. **79**, 153–162 (2012).
[84]T. B. Schrøder, N. P. Bailey, U. R. Pedersen, N. Gnan, and J. C. Dyre, J. Chem. Phys. **131**(23), 234503 (2009).
[85]N. Gnan, T. B. Schrøder, U. R. Pedersen, N. P. Bailey, and J. C. Dyre, J. Chem. Phys. **131**(23), 234504 (2009).
[86]R. Sharma, M. Agarwal, and C. Chakravarty, Mol. Phys. **106**(15), 1925–1938 (2008).
[87]M. Agarwal, M. Singh, R. Sharma, M. Parvez Alam, and C. Chakravarty, J. Phys. Chem. B **114**(20), 6995–7001 (2010).
[88]M. Agarwal, M. P. Alam, and C. Chakravarty, J. Phys. Chem. B **115**(21), 6935–6945 (2011).
[89]H. S. Green, *The Molecular Theory of Fluids* (North-Holland, Amsterdam, 1952).
[90]D. C. Wallace, Phys. Lett. A **122**(8), 418–420 (1987).
[91]D. C. Wallace, J. Chem. Phys. **87**(4), 2282–2284 (1987).
[92]D. C. Wallace, Phys. Rev. A **39**(9), 4843 (1989).
[93]D. C. Wallace, Proc. R. Soc. London, Ser. A **433**(1889), 615–630 (1991).
[94]H. J. Raveché, J. Chem. Phys. **55**(5), 2242–2250 (1971).
[95]A. Baranyai and D. J. Evans, Phys. Rev. A **40**(7), 3817 (1989).
[96]J.-L. Bretonnet, J. Chem. Phys. **117**(20), 9370–9373 (2002).
[97]T. Goel, C. N. Patra, T. Mukherjee, and C. Chakravarty, J. Chem. Phys. **129**(16), 164904 (2008).
[98]R. Chopra, T. M. Truskett, and J. R. Errington, J. Phys. Chem. B **114**(49), 16487–16493 (2010).
[99]G. Galliero, C. Boned, and J. Fernández, J. Chem. Phys. **134**(6), 064505 (2011).
[100]B. S. Jabes and C. Chakravarty, J. Chem. Phys. **136**(14), 144507 (2012).
[101]R. D. Mountain and H. J. Raveché, J. Chem. Phys. **55**(5), 2250–2255 (1971).
[102]I. Borzsák and A. Baranyai, Chem. Phys. **165**(2–3), 227–230 (1992).
[103]B. B. Laird and A. D. J. Haymet, Phys. Rev. A **45**(8), 5680 (1992).
[104]F. Saija, A. M. Saitta, and P. V. Giaquinta, J. Chem. Phys. **119**(7), 3587–3589 (2003).
[105]Z. Yan, S. V. Buldyrev, and H. E. Stanley, Phys. Rev. E **78**(5), 051201 (2008).
[106]Y. D. Fomin and V. N. Ryzhov, Phys. Lett. A **375**(22), 2181–2184 (2011).
[107]D. Dhabal, A. H. Nguyen, M. Singh, P. Khatua, V. Molinero, S. Bandyopadhyay, and C. Chakravarty, J. Chem. Phys. **143**(16), 164512 (2015).
[108]J. Zielkiewicz, J. Phys. Chem. B **112**(26), 7810–7815 (2008).
[109]T. Lazaridis and M. Karplus, J. Chem. Phys. **105**(10), 4294–4316 (1996).
[110]T. Lazaridis, J. Phys. Chem. B **104**(20), 4964–4979 (2000).
[111]A. Kuffel and J. Zielkiewicz, J. Phys. Chem. B **116**(40), 12113–12124 (2012).
[112]A. Kuffel, D. Czapiewski, and J. Zielkiewicz, J. Chem. Phys. **141**(5), 055103 (2014).
[113]P. Kumar, S. V. Buldyrev, and H. E. Stanley, Proc. Natl. Acad. Sci. U. S. A. **106**(52), 22130–22134 (2009).
[114]J. Zielkiewicz, J. Chem. Phys. **123**(10), 104501 (2005).
[115]J. Zielkiewicz, J. Chem. Phys. **128**(19), 196101 (2008).
[116]L. Wang, R. Abel, R. A. Friesner, and B. J. Berne, J. Chem. Theory Comput. **5**(6), 1462–1473 (2009).
[117]E. Giuffré, S. Prestipino, F. Saija, A. M. Saitta, and P. V. Giaquinta, J. Chem. Theory Comput. **6**(3), 625–636 (2010).
[118]S.-T. Lin, M. Blanco, and W. A. Goddard III, J. Chem. Phys. **119**(22), 11792–11805 (2003).
[119]S.-T. Lin, P. K. Maiti, and W. A. Goddard III, J. Phys. Chem. B **114**(24), 8191–8198 (2010).
[120]T. A. Pascal, S.-T. Lin, and W. A. Goddard III, Phys. Chem. Chem. Phys. **13**(1), 169–181 (2011).
[121]J. Jin and W. A. Goddard III, J. Phys. Chem. C **119**(5), 2622–2629 (2015).
[122]W. A. Goddard, *Computational Materials, Chemistry, and Biochemistry: From Bold Initiatives to the Last Mile* (Springer, 2021), pp. 1089–1095.
[123]T. Sun, J. Xian, H. Zhang, Z. Zhang, and Y. Zhang, J. Chem. Phys. **147**(19), 194505 (2017).
[124]S. S. Pannir Sivajothi, S.-T. Lin, and P. K. Maiti, J. Phys. Chem. B **123**(1), 180–193 (2018).
[125]R. A. X. Persson, V. Pattni, A. Singh, S. M. Kast, and M. Heyden, J. Chem. Theory Comput. **13**(9), 4467–4481 (2017).
[126]V. Pattni, T. Vasilevskaya, W. Thiel, and M. Heyden, J. Phys. Chem. B **121**(31), 7431–7442 (2017).
[127]M. Heyden, Wiley Interdiscip. Rev.: Comput. Mol. Sci. **9**(2), e1390 (2019).
[128]J. Jin, A. J. Pak, and G. A. Voth, J. Phys. Chem. Lett. **10**(16), 4549–4557 (2019).
[129]R. Palomar and G. Sesé, J. Chem. Phys. **148**(8), 084504 (2018).
[130]D. A. McQuarrie and J. D. Simon, *Physical Chemistry: A Molecular Approach* (University Science Books, Sausalito, CA, 1997).
[131]R. L. Henderson, Phys. Lett. A **49**(3), 197–198 (1974).
[132]W. G. Noid, Methods Mol. Biol. **924**, 487–531 (2013).
[133]J. W. Wagner, J. F. Dama, A. E. P. Durumeric, and G. A. Voth, J. Chem. Phys. **145**(4), 044108 (2016).
[134]A. K. Soper, J. Chem. Phys. **101**(8), 6888–6901 (1994).
[135]G. R. Medders, V. Babin, and F. Paesani, J. Chem. Theory Comput. **9**(2), 1103–1114 (2013).
[136]G. A. Cisneros, K. T. Wikfeldt, L. Ojamäe, J. Lu, Y. Xu, H. Torabifard, A. P. Bartók, G. Csányi, V. Molinero, and F. Paesani, Chem. Rev. **116**(13), 7501–7528 (2016).
[137]F. H. Stillinger and T. A. Weber, Phys. Rev. B **31**(8), 5262 (1985).
[138]V. Molinero and E. B. Moore, J. Phys. Chem. B **113**(13), 4008–4016 (2008).
[139]C. Scherer and D. Andrienko, Phys. Chem. Chem. Phys. **20**(34), 22387–22394 (2018).
[140]L. Larini, L. Lu, and G. A. Voth, J. Chem. Phys. **132**(16), 164107 (2010).
[141]J. J. Hoyt, M. Asta, and B. Sadigh, Phys. Rev. Lett. **85**(3), 594 (2000).
[142]Y. D. Fomin, V. Ryzhov, and N. Gribova, Phys. Rev. E **81**(6), 061201 (2010).
[143]J. Jin, Y. Han, A. J. Pak, and G. A. Voth, J. Chem. Phys. **154**(4), 044104 (2021).
[144]J. Jin, A. J. Pak, Y. Han, and G. A. Voth, J. Chem. Phys. **154**(4), 044105 (2021).
[145]J. Yvon, *La théorie statistique des fluides et l'équation d'état* (Hermann & Cie, 1935).
[146]J. G. Kirkwood, J. Chem. Phys. **14**(3), 180–201 (1946).
[147]M. Born and H. Green, Proc. R. Soc. London, Ser. A **188**(1012), 10–18 (1946).
[148]N. Bogolubov, Zh. Eksp. Teor. Fiz. **16**(8), 691–702 (1946).
[149]J. G. Kirkwood, F. P. Buff, and M. S. Green, J. Chem. Phys. **17**(10), 988–994 (1949).
[150]S. Izvekov and G. A. Voth, J. Chem. Phys. **123**(13), 134105 (2005).
[151]S. Izvekov and G. A. Voth, J. Phys. Chem. B **109**(7), 2469–2473 (2005).
[152]W. G. Noid, J.-W. Chu, G. S. Ayton, V. Krishna, S. Izvekov, G. A. Voth, A. Das, and H. C. Andersen, J. Chem. Phys. **128**(24), 244114 (2008).

[153]W. G. Noid, P. Liu, Y. Wang, J.-W. Chu, G. S. Ayton, S. Izvekov, H. C. Andersen, and G. A. Voth, J. Chem. Phys. **128**(24), 244115 (2008).
[154]L. Lu, S. Izvekov, A. Das, H. C. Andersen, and G. A. Voth, J. Chem. Theory Comput. **6**(3), 954–965 (2010).
[155]J. Jin, A. Yu, and G. A. Voth, J. Chem. Theory Comput. **16**(11), 6823–6842 (2020).
[156]S. Plimpton, J. Comput. Phys. **117**, 1–19 (1995).
[157]W. M. Brown, P. Wang, S. J. Plimpton, and A. N. Tharrington, Comput. Phys. Commun. **182**(4), 898–911 (2011).
[158]W. M. Brown, A. Kohlmeyer, S. J. Plimpton, and A. N. Tharrington, Comput. Phys. Commun. **183**(3), 449–459 (2012).
[159]H. J. C. Berendsen, J. R. Grigera, and T. P. Straatsma, J. Phys. Chem. **91**(24), 6269–6271 (1987).
[160]Y. Wu, H. L. Tepper, and G. A. Voth, J. Chem. Phys. **124**(2), 024503 (2006).
[161]J. L. F. Abascal and C. Vega, J. Chem. Phys. **123**(23), 234505 (2005).
[162]J. L. F. Abascal, E. Sanz, R. García Fernández, and C. Vega, J. Chem. Phys. **122**(23), 234511 (2005).
[163]W. L. Jorgensen, D. S. Maxwell, and J. Tirado-Rives, J. Am. Chem. Soc. **118**(45), 11225–11236 (1996).
[164]G. A. Kaminski, R. A. Friesner, J. Tirado-Rives, and W. L. Jorgensen, J. Phys. Chem. B **105**(28), 6474–6487 (2001).
[165]S. Nosé, J. Chem. Phys. **81**(1), 511–519 (1984).
[166]W. G. Hoover, Phys. Rev. A **31**(3), 1695 (1985).
[167]H. C. Andersen, J. Chem. Phys. **72**(4), 2384–2393 (1980).
[168]A. Das, L. Lu, H. C. Andersen, and G. A. Voth, J. Chem. Phys. **136**(19), 194115 (2012).
[169]L. Lu and G. A. Voth, J. Chem. Phys. **134**(22), 224107 (2011).
[170]T. T. Foley, M. S. Shell, and W. G. Noid, J. Chem. Phys. **143**(24), 243104 (2015).
[171]K. M. Lebold and W. G. Noid, J. Chem. Phys. **150**(1), 014104 (2019).
[172]K. M. Lebold and W. G. Noid, J. Chem. Phys. **151**(16), 164113 (2019).
[173]M. P. Allen and D. J. Tildesley, *Computer Simulation of Liquids* (Oxford University Press, 2017).
[174]E. Herbst, J. K. Messer, F. C. De Lucia, and P. Helminger, J. Mol. Spectrosc. **108**(1), 42–57 (1984).
[175]J. Jin, Y. Han, and G. A. Voth, J. Chem. Theory Comput. **14**(12), 6159–6174 (2018).
[176]J. Jin, K. S. Schweizer, and G. A. Voth, J. Chem. Phys. **158**, 034104 (2023); arXiv:2208.01257.